Excision of uracil from DNA by hSMUG1 includes strand incision and processing

Marina Alexeeva[1, §], Marivi N. Moen[1,2, §], Kristin Grøsvik[1], Almaz N. Tesfahun[1], Xiang Ming Xu[1], Izaskun Muruzábal-Lecumberri[1], Kristine M. Olsen[1], Anette Rasmussen[3], Peter Ruoff[1], Finn Kirpekar[3], Arne Klungland[2,4] and Svein Bjelland[1,*]

[1]Department of Chemistry, Bioscience and Environmental Technology-Centre for Organelle Research, Faculty of Science and Technology, University of Stavanger, P.O. Box 8600 Forus, N-4021 Stavanger, Norway

[2]Department of Microbiology, Oslo University Hospital, Rikshospitalet, NO-0372 Oslo, Norway

[3]Department of Biochemistry and Molecular Biology, University of Southern Denmark, 5230 Odense M, Denmark

[4]Department of Molecular Medicine, Institute of Basic Medical Sciences, University of Oslo, NO-0317 Oslo, Norway

* To whom correspondence should be addressed. Tel: +47 51831884/+47 47286404; Email: svein.bjelland@uis.no

[§]The authors wish it to be known that, in their opinion, the first 2 authors should be regarded as joint First Authors.

ABSTRACT

Uracil (U) arises in DNA by hydrolytic deamination of cytosine (C) and by erroneous incorporation of deoxyuridine monophosphate opposite adenine, where the former event is devastating by generation of C → thymine transitions. The base excision repair (BER) pathway replaces uracil by the correct base. In human cells two uracil-DNA glycosylases (UDGs) initiate BER by excising uracil from DNA; one is hSMUG1 (human single-strand-selective mono-functional UDG). We report that repair initiation by hSMUG1 involves strand incision at the uracil site resulting in a 3´-α,β-unsaturated aldehyde designated uracil-DNA incision product (UIP), and a 5´-phosphate. UIP is removed from the 3´-end by human apurinic/apyrimidinic (AP) endonuclease 1 preparing for single-nucleotide insertion. hSMUG1 also incises DNA or processes UIP to a 3´-phosphate designated uracil-DNA processing product (UPP). UIP and UPP were indirectly identified and quantified by polyacrylamide gel electrophoresis and chemically characterised by matrix-assisted laser desorption/ionisation time-of-flight mass-spectrometric analysis of DNA from enzyme reactions using ^{18}O- or ^{16}O-water. The formation of UIP accords with an elimination (E2) reaction where deprotonation of C2´ occurs via the formation of a C1´ enolate intermediate. A three-phase kinetic model explains rapid uracil excision in phase 1, slow unspecific enzyme adsorption/desorption to DNA in phase 2 and enzyme-dependent AP site incision in phase 3.

INTRODUCTION

Although uracil (U) formed by deamination of cytosine (C) is most harmful to cell function due to formation of C → thymine (T) transition mutations (1,2), which are the most common spontaneous mutation in cells frequently found in human tumours (3), uracil is also incorporated into DNA opposite adenine (A) through deoxyuridine triphosphate (dUTP) which has escaped dUTPase digestion (4). Uracil in DNA is repaired by the base excision repair (BER) pathway (5,6) initiated by a uracil-DNA glycosylase (UDG; EC 3.2.2.27), constituting the UDG superfamily (7) sharing gross architecture and organisation of the active site. The major and most effective UDG for removal of uracil from nuclear DNA in human cells is hUNG2, while hUNG1 is the mitochondrial splice variant (family 1 UDG). It is believed to be responsible for both pre-replicative removal of deaminated cytosine [U opposite guanine (G)], post-replicative removal of mis-incorporated uracil (U opposite A) at the replication fork, as well as removal of deaminated cytosine outside of replication foci. In contrast, hSMUG1 (human single-strand-selective mono-functional UDG; family 3 UDG) (8) has been proposed the role as a backup UDG in the absence of hUNG (9), as well as it has a broader substrate specificity removing pyrimidines damaged by oxidation like 5-hydroxyuracil, 5-hydroxymethyluracil, 5-formyluracil and 5-carboxyuracil in addition to 5-fluorouracil (10-13). Thus, hUNG exhibits a strict active site which is nearly specific for uracil while that of hSMUG1 is relaxed (14,15). While hUNG is upregulated during S-phase and binds to the replication clamp [PCNA (proliferating cell nuclear antigen)] to efficiently remove U opposite G (and A) before mutation fixation by the replicative polymerase, hSMUG1 is a constitutive enzyme to initiate BER in non-replicating cells (9,16). While hUNG rapidly leaves the apurinic/apyrimidinic (AP) site for human AP endonuclease 1 (hAPE1), hSMUG1 competes with hAPE1 for AP site-binding to slowly be replaced by hAPE1 (17). Indeed, as opposed to hUNG and contradicting its name, hSMUG1 interacts with both DNA strands where a specific interaction with G opposite an AP site strengthen the binding (17-19). Especially important for higher vertebrates is the involvement of hUNG in immunoglobulin diversification (20), where many molecular details including the participation of hSMUG1 still need to be more thoroughly defined (21,22).

Hitherto, all UDGs including the human family 2 UDG designated thymine-DNA glycosylase (23), because of its involvements in other cellular functions than uracil repair (24,25), have been described as mono-functional enzymes depending on downstream BER proteins for AP site-incising and excising functions (26). In contrast, bi-functional DNA glycosylases have additional lyase activity carrying out a β- or β/δ-elimination reaction to incise the AP site, although the latter reaction is believed to predominantly being accomplished by hAPE1 (27,28). The 3′-deoxyribose phosphate (dRP) and 3′-α,β-unsaturated aldehyde remnants after the β-elimination reaction are also removed by the 3′-phosphodiesterase function of hAPE1 (29), whereas the 3′-phosphate left after the β/δ-elimination reaction is removed by the human polynucleotide kinase phosphatase (hPNKP) (2). The BER pathway is completed by the sequential action of DNA polymerase β (30), which also removes the 5′-dRP by its lyase function if hAPE1 incised the AP site, and DNA ligase (1,2,6).

Following damaged base removal, DNA glycosylases bind the resulting AP site with different strengths to protect it from premature hydrolytic cleavage that may cause DNA strand breakage and

collapse. This also contributes to recruit downstream BER proteins to the lesion site. Since hSMUG1, as mentioned above, binds the AP site much stronger than hUNG (18), we asked the question whether its active site residues causing glycosidic bond cleavage may come in position to react with AP site atoms. Indeed, here we show that exposure of DNA oligomers with deoxyuridine monophosphate (dUMP) incorporated at a specific site (U-DNA) to hSMUG1 causes strand cleavage at the lesion site, indicating that the enzyme incises DNA after uracil removal. However, since the AP site is labile in water solutions, we determined its rate of cleavage in different buffers at different temperatures, and eventually quantified the non-enzymatic incision of hSMUG1-generated AP sites during the high-temperature sample preparation for denaturing polyacrylamide gel electrophoresis (PAGE). Moreover, we measured hSMUG1-mediated incision of U-DNA in the absence of high temperature. The incision products were indirectly identified and quantitated by PAGE, and chemically identified by matrix-assisted laser desorption/ionisation (MALDI) time-of-flight (TOF) mass spectrometric (MS) analysis of DNA from enzyme reactions in the presence of ^{18}O- or ^{16}O-water. We developed a model describing the kinetics of the U-DNA incision activity, which accords with known characteristics for hSMUG regarding uracil excision and DNA binding, and suggest a novel catalytic mechanism for DNA strand incision by glycosylases.

MATERIAL AND METHODS

Oligonucleotide substrates

Single-stranded DNA (ssDNA) with uracil at a specific site protected by phosphorothioate (four bonds) at each end were supplied with synthetically incorporated Cy3 fluorophore (or without it when labelled with [γ-^{32}P]ATP) by Sigma or Eurofins MWG: 5´-TAGACATTGCCCTCGAGGTAUCATGGATCCGATTTCGACCTCAAACCTAGACGAATTCC G-3´ [60 nucleotides (nt); to prepare substrate 1]; 5´-[Cy3]-CCCTCGAGGTAUCATGGATCCGATCG -3´ (26 nt; to prepare substrate 2). Equimolar amounts of the labelled and complementary strands were annealed, with U opposite G, respectively, by heating at 95 °C for 4 min followed by cooling to room temperature for 2 h. For MS analyses, substrate 2 (unlabelled) from Sigma and Eurofins MWG was not protected with phosphorothioate.

Enzymes

hSMUG1 (full length) was obtained from NEB (New England BioLabs) and investigated for contaminants by MS analysis (see Supplementary Data, Table S1) as well as purified by us [see Supplementary Data, *Production of purified hSMUG1(25–270)* and Figure S2]. EcUng was obtained from NEB, Fermentas and Trevigen; EcNfo was obtained from Fermentas; EcFpg, EcNth, hOGG1 and hAPE1 were obtained from NEB; hUNG (hUNGΔ84 with/without His-tag) (9,31) was a gift from B. Kavli and G. Slupphaug.

Assays for incision of U-DNA

Purified protein was incubated with U-DNA (substrate 1or 2) in 45 mM HEPES [4-(2-hydroxyethyl)-1-piperazineethanesulphonic acid]-KOH, pH 7.8, 0.4 mM ethylenediaminetetraacetic acid (EDTA), 1 mM dithiothreitol (DTT), 70 mM KCl, 2% (v/v) glycerol (reaction buffer) at 37 °C (final volume, 20 µl), unless otherwise stated. To convert U-DNA into AP-DNA, either substrate 1 (0.5 pmol) or substrate 2 (1 pmol) was incubated with EcUng (1 pmol) for 20 min using the same conditions. Reactions were terminated by the addition of 20 mM EDTA, 0.5% (w/v) sodium dodecyl sulphate (SDS) and proteinase K (190 µg/ml) followed by precipitation of DNA with 96% ethanol containing 0.1 M sodium acetate supplemented with 16 µg tRNA followed by solubilisation in water (10 µl) (32). Enzymatic excision of uracil, which results in an alkali-labile AP site, was monitored in parallel by the extent NaOH (0.1 M final concentration) cleaved the DNA after 10 min at 90 °C (33). Samples (10 µl) were added 10 µl of a loading solution containing 80% (v/v) formamide, 1 mM EDTA and 0.05% (w/v) xylene cyanol, and in the initial experiments following the conventional procedure, incubated at 95 °C for 5 min to denature DNA (Figure 1A). After cooling on ice, a portion of each sample (5 µl) was analysed by denaturing PAGE [20% (w/v) polyacrylamide gels with 7 M urea; see Figure 1B]. To measure non-enzymatic incision of AP-DNA in different solutions at different times and temperatures, we used the same conditions and/or procedure (see Figure 2A). To eliminate non-enzymatic cleavage of AP sites, the samples (10 µl; DNA dissolved in water) were treated at room temperature instead of 95 °C, and following addition of the loading solution referred to above (10 µl) subjected to PAGE without delay, where the gel [20% (w/v)] contained 3% (v/v) formamide instead of urea (see Figure 4A). However, in the experiments determining the relative migration of the different 3´-end products, the PAGE gel [20% (w/v)] contained 7 M urea (see Figure 7). Visualisation and quantification were performed by fluorescence or phosphor imaging analysis using ImageQuant Software (Molecular Dynamics Inc.). The graphs were drawn using KaleidaGraph version 4.1.0 (Synergy Software).

Trapping experiment for Schiff base intermediate

The assay was performed according to Zharkov *et al.* (34). Polydeoxynucleotide duplex containing a single U residue opposite G (substrate 2, 1 pmol) was incubated with enzyme (see Figure 6) and freshly dissolved 50 mM $NaBH_4$ in reaction buffer at 37 °C for 1 h (final volume, 10 µl). Reaction was terminated by the addition of 10 µl of DNA denaturing loading buffer (80 % formamide, 1 mM EDTA, 0.05 % (w/v) bromophenol blue) and boiled at 95°C for 5 min before loading into a 10% (w/v) denaturing PAGE gel. The gels were scanned using Typhoon Trio Imager (GE Healthcare). Visualization and quantification were performed by phosphor imaging analysis using ImageQuant Software (Molecular Dynamics Inc.).

MALDI-TOF-MS analysis of U-DNA digested by hSMUG1 in normal water or $H_2{}^{18}O$

Reaction mixtures containing hSMUG1 (0.3 pmol) together with (re-suspended) unlabelled substrate 2 (normal $H_2{}^{16}O$ experiments, 10 pmol; $H_2{}^{18}O$ experiments, 20 pmol) were incubated in 20 mM Tris-HCl, pH 8.0, 1 mM DTT, 1 mM EDTA, 70 mM KCl at 37 °C for 30 min (normal $H_2{}^{16}O$ experiments; final volume, 20 µl), or 1 h ($H_2{}^{18}O$ experiments; final volume, 10 µl), if not otherwise stated. Control incubations were performed with EcUng (0.78 pmol) plus either hOGG1 (13 pmol), EcNth (8.7 pmol)

or EcFpg (17 pmol) to compare the hSMUG1-generated 3´-end product with those of characterised enzymes. MALDI-TOF-MS analyses on reaction products were carried out as described (35). Substrate DNA was evaporated using vacuum centrifugation followed by re-suspension in $H_2{}^{18}O$ (Aldrich, Product No. 329878; 20 µl). The ^{18}O-labelling of the enzymatic products was performed by dissolving them in $H_2{}^{18}O$ followed by incubation at 4 °C overnight. The MS was performed as above, but with $H_2{}^{18}O$ replacing $H_2{}^{16}O$ in every step. DNA was precipitated with 96% ethanol, 1 M ammonium acetate and 0.1 µg/µl glycogen followed by incubation at -20 °C overnight (for some experiments precipitation was performed as in the experiments using PAGE as described above). DNA pellet was collected by centrifugation at 13,000 rpm for 30 min at 4 °C.

Kinetic model calculations

From the calculated concentration [P1] (see Figure 9A) the reaction velocity for the 20 min assay was calculated as

$$V^{in} = [P1]_{20}/20 \text{ (nM/min)}$$

where $[P1]_{20}$ denotes the concentration of P1 after 20 min. The rate equations of the model were solved numerically by using the Fortran subroutine LSODE (36) in conjunction with Absoft's Pro Fortran compiler (www.absoft.com) with a (model) simulation time of 20 min. From the numerical output, graphs were constructed showing V^{in} in nM/min as a function of the enzyme concentration $[E]_0$ (in nM). For the time-dependent graphs, the concentration-time data for the formation of the incision product P1, the excision product U and substrate DNA (S), were extracted from our previous calculation at the initial $[E]_0$ concentrations of 0.05, 0.1, 0.15, 0.2, and 0.25 nM. Plots were generated using gnuplot (www.gnuplot.info) and Adobe Illustrator (www.adobe.com). A detailed description of the model is presented in the Supplementary Data (see *A three-phase kinetic model*).

RESULTS

The presence of hSMUG1 causes cleavage of U-DNA into two different 3´-end products

A common method to determine DNA glycosylase activity employs an oligodeoxyribonucleotide with the damaged base residue (*in casu*, a uracil) inserted at a specific position. Enzymatic excision of uracil results in an alkali-labile AP site, which can be monitored by the extent that *e.g.* NaOH cleaves such sites by a β/δ-elimination reaction (37), where cleaved DNA is separated from un-cleaved DNA by PAGE under denaturing conditions (Figure 1A). We incubated such substrate, fluorescently labelled at the 5´ end of the damaged strand (substrate 1), with increasing amounts of hSMUG1. Apparently, protein-dependent cleavage of the DNA at the lesion site took place without alkali (Figure 1B, lanes 4–7), although less than in the samples treated with NaOH (Figure 1B, lanes 8–10). Repeated experiments using different enzyme preparations demonstrated that hSMUG1 removed virtually all uracil residues present in the DNA at the highest protein concentration examined, whereas total strand incision ceased when about ⅔ of the uracils had been removed (Figure 1C). Neither U-DNA incision nor uracil excision occurred without enzyme (Figure 1B, lanes 2 and 3, respectively). It is also important to note, that we always employed reaction conditions without Mg^{2+} and with EDTA

added, to minimise possible contaminating AP endonuclease activity (2), in spite of the fact that UDGs are stimulated by Mg^{2+} ions (9). In conclusion, hSMUG1 seemed to incise U-DNA at the lesion site.

The major 3´-product generated in the presence of hSMUG1 without alkali treatment, hereafter designated U-DNA incision product (UIP), migrated more slowly than the 3´-phosphate/δ-elimination product formed by NaOH/heat treatment of AP-DNA (Figure 1B). In addition, a product migrating like the 3´-phosphate appeared at higher hSMUG1 concentrations and was designated U-DNA processing product (UPP) (Figure 1B).

AP-DNA converts efficiently to UIP at increased temperatures, which can explain one third of the UIP formed from U-DNA in the presence of hSMUG1

The method employed to determine UDG activity (Figure 1A) is indirect but quantitative since uracil is a stable base in DNA and virtually all AP sites generated is a result of uracil excision. The AP site generated by UDG and other DNA glycosylases is chemically indistinguishable from the AP site formed in cellular DNA by hydrolytic depurination/depyridination (38-40), where the latter is the most abundant DNA lesion in all cells (6). However, this common or normal AP site (as opposed to *e.g.* oxidised or reduced AP sites) is chemically relatively unstable, also at physiological pH, leading to DNA chain breakage (41). Since this instability increases greatly with temperature, and we denatured the hSMUG1-exposed DNA oligomer for 5 min at 95 °C in the presence of formamide to prepare for PAGE (Figure 1A), another possible explanation for the U-DNA incision observed (Figure 1B) is non-enzymatic AP site cleavage caused by this heat treatment (39). Importantly, while NaOH/heat cleaves the AP site into a 3´-phosphate by β/δ-elimination (40), it has previously been shown that the 3´-product formed by thermolysis of AP sites at neutral pH is an α,β-unsaturated aldehyde (39). This could imply that the increase in DNA cleavage as a function of increasing protein concentration only reflected the appearance of an increasing number of AP sites made by the increasing amount of hSMUG1 added. Since such non-enzymatic hydrolysis would be a time-dependent process, U-DNA (substrates 1) was pre-treated with *Escherichia coli* family 1 UDG (EcUng), commonly used for this purpose, to convert the uracil residues into AP sites (Figure 2A). Then, the resulting AP-DNA was exposed to 95 °C for different time-periods in the formamide-containing solution employed to denature DNA for PAGE. Parallel samples were also NaOH/heat-treated to determine the amount of AP sites in the substrate (Figure 2B, lane 1). The results show that such non-enzymatic AP site cleavage was significant at 95 °C during the 30 min period investigated (Figure 2B, lanes 2–7), where about 80% of the AP-DNA was converted to 3´-α,β-unsaturated aldehyde while < 10% to 3´-phosphate/UPP (Figure 2C). Comparing the hSMUG1-incised U-DNA with the 5 min-treated AP-DNA indicates a more efficient generation of UIP from U-DNA by the highest amount of hSMUG1 (Figure 1B, lane 7) than of the 3´-α,β-unsaturated aldehyde from AP-DNA by heat (Figure 2B, lane 4). Indeed, both incision of U-DNA with hSMUG1 (Figure 1B) and cleavage of AP-DNA by heat (Figure 2B) show just one clear band at the position of UIP or the 3´-α,β-unsaturated aldehyde in PAGE, suggesting that they are chemically identical. Repeated experiments showed an initial rate of incision of ~4% of the total

amount of AP sites in the DNA per min at 95 °C (Figure 2C). AP-DNA was also exposed to 10 mM Tris, pH 7.5, 1 mM EDTA (TE) and pure water, to investigate whether buffer/solution composition is important for cleavage. The results show that AP-DNA was cleaved similarly in all these three solutions, which amounted to an initial rate of 3.8 ± 0.2% of the total AP sites in the substrate per min (Figure 2D). At 75 °C the initial cleavage rate was 0.74 ± 0.02% of the total AP sites in the substrate per min (Figure 2E), also with no difference between the formamide and water solutions. Moreover, at 75 °C only UIP (and no UPP) appeared as cleavage product (Figure 2C and data not shown). Importantly, experiments performed at 37 °C using the same conditions as above showed no significant cleavage of AP-DNA (Figure 2C). In conclusion, our experiments show that non-enzymatic hydrolysis of AP-DNA at neutral pH increases significantly with temperature and generates the 3´-α,β-unsaturated aldehyde as cleavage product, which accords with previous results (39). The effect of the buffer composition seemed to be minimal. We only observed UPP as a minor product arising at 95 °C (Figure 2C).

The significant hydrolysis of AP sites to the 3´-α,β-unsaturated aldehyde at 95 °C, which migrated in PAGE as UIP (Figure 2B), seemed to challenge the interpretation of the original experiments which indicated hSMUG1-catalysed incision of U-DNA at the lesion site (Figure 1B). However, this chemical decay of (hSMUG1-generated) AP sites during the 5 min heat treatment for sample preparation was easily measured and quantified to 19.2 ± 0.8% of the total number of AP sites in the sample DNA (Figure 2D); the latter measured by NaOH/heat-mediated cleavage of product DNA exposed to each hSMUG1 concentration. Since we routinely analysed samples treated with and without NaOH in parallel (Figure 1A), the number quoted was calculated from the former to be subtracted from the latter. As stated in the previous section, no separation of the chemically formed 3´-α,β-unsaturated aldehyde and the “enzymatically” formed UIP was ever observed (Figure 1B and data not shown) indicating molecular identity. Thus, the apparent incision measured as increasing as a function of hSMUG1 concentration [Figure 1C; U-DNA incision (total)] had to be adjusted for this non-enzymatic background incision to show the true estimate of the hSMUG1-catalysed protein-dependent incision of U-DNA [Figure 1C; U-DNA incision (enzymatic)]. This was only about 2 or 3 times lower than the uracil excision at comparable enzyme concentrations.

Indirect identification and the time-dependent formation of UIP and UPP from U-DNA in the presence of hSMUG1

At the beginning of our study we observed (Figure 1B) that UIP migrated more slowly during PAGE than the 3´-phosphate formed by NaOH-mediated incision of AP sites (37). UIP also seemed to migrate like the 3´-product formed by non-enzymatic hydrolysis of AP sites in the presence of formamide at high temperature (Figure 2B), previously identified as 3´-α,β-unsaturated aldehyde (39). In contrast, UPP migrated like 3´-phosphate (Figure 1B). To try identifying both species, U-DNA exposed to hSMUG1 for different time periods was analysed together with 3´-incision products made by other known AP site-incising enzymes under PAGE conditions favouring separation of different end products, which has been a common method to identify the nature of such DNA ends resulting

from incision of AP sites by BER enzymes. To increase the visibility and amount of UPP, which in our first experiments appeared as a minor product (Figure 1B), the U-DNA was radioactively labelled. To make chemically characterised 3´-end products, U-DNA (substrate 1) was pre-treated with EcUng to convert uracil into an AP site followed by treatment with either a) *E. coli* endonuclease III (EcNth) to define a 3´-dRP formed by β-elimination (42), b) *E. coli* endonuclease IV (EcNfo) to define a 3´-OH (43), c) *E. coli* formamidopyrimidine-DNA glycosylase (EcFpg) (44) to define a 3´-phosphate formed by β/δ-elimination (δ-product; also formed by NaOH/heat as mentioned above) or d) human 8-oxoguanine-DNA glycosylase (hOGG1) to define the 3´-α,β-unsaturated aldehyde (42,44). As expected, the result showed that UIP migrated differently from the products defined by the enzymes EcNth, EcNfo and EcFpg, but identical to the product formed by hOGG1 (Figure 3A), *i.e.*, like the 3´-α,β-unsaturated aldehyde. Since, as indicated before, this product also is formed by thermolysis of AP sites at neutral pH (39), the result can explain our observations. As expected, also UPP migrated differently from the products defined by the enzymes EcNth, EcNfo and hOGG1, but identical to the product formed by EcFpg, *i.e.*, like a 3´-phosphate (Figure 3A).

Besides indicating the chemical nature of UIP and UPP, the experiment presented in Figure 3A also shows significant formation of UPP by prolonged incubation with hSMUG1, becoming similarly abundant as UIP after incubation for 30 min (lanes 8 and 9). Indeed, after 90 min UPP was twice as abundant as UIP (Figure 3B). This contrasts with the negligible amount of UPP formed by thermal degradation of AP-DNA even at the highest temperature examined, with ~1% after 10 min and ~6% after 30 min at 95 °C (Figure 2C). Thus, sample preparation for 5 min at 95 °C should hardly form detectable amounts of UPP (Figures 2B and 2C). This accords with the above cited results which identified UIP/3´-α,β-unsaturated aldehyde as the major product generated by thermolysis at neutral pH, and also showed that UIP needs prolonged incubation at high temperature to be converted significantly to UPP (39). Since the efficient formation of UPP in the presence of hSMUG1 (Figure 3) cannot be explained by thermolysis of AP sites or UIP, the only interpretation left is that it is generated by hSMUG1; either as a second “U-DNA incision product” or by processing of UIP. When U-DNA pre-incised by hSMUG1 was incubated with hAPE1, all UIP converted into 3´-OH product (Supplementary Data, Figure S1), showing that UIP is processed by the BER pathway.

U-DNA incision by hSMUG1 confirmed under conditions of no significant spontaneous AP-DNA incision

To minimise spontaneous incision of AP sites in DNA during sample preparation for denaturing PAGE, we decided to try avoiding exposure to high temperature and instead treat the enzymatically exposed DNA (substrate 1) with PAGE loading solution/formamide at room temperature, in addition to adding formamide to the gel (Figure 4A). Using no temperature above 37 °C, hydrolytic incision of AP sites should be minimal (Figure 2C). Somewhat surprising, the result showed that this treatment was sufficient to release the 20 nt 5´-incision product from the un-incised DNA (Figure 4B), confirming the ability of hSMUG1 to cleave DNA at the uracil site in a protein-dependent manner (Figure 4C).

hSMUG1 was also incubated with single-stranded U-DNA (ssU-DNA; the labelled strand of substrate 1; Figure 1A) under similar conditions as described above for double-stranded DNA (dsDNA). The result showed that the enzyme incised ssU-DNA (Figure 5A) in a protein-dependent manner within the same order of magnitude (Figure 5B) as dsDNA (Figure 4C). This differs from AP lyases which exhibit low activity for dsDNA (2), thus minimising suspicion of contamination of the hSMUG1 preparation by such activity.

Confirmation of hSMUG1 incision activity by freshly prepared enzyme preparation using different buffers

To improve the experimental evidence for the novel hSMUG1 enzyme functions, we overexpressed a truncated version of the human *smug1* gene and purified the corresponding catalytically active hSMUG(25–270) protein [Supplementary Data, *Production of purified hSMUG1(25–270)* and Figure S2]. The results confirmed the previous findings by demonstrating a U-DNA incision and processing activity and uracil excision activity of hSMUG(25–270) (Figures 4D and 4E) similar to the commercial hSMUG1 preparation (Figures 4B and 4C). Considering the higher amounts of enzyme used and the double incubation time the UPP clearly appears in addition to UIP (Figure 4D) as opposed to the other case only showing one product band corresponding to UIP (Figure 4B). The U-DNA incision (comprising both UIP and UPP) as compared to the uracil excision is also higher with hSMUG(25–270) (Figure 4E) than with commercial hSMUG1 (Figure 4C). Besides, the presence of amines in the (HEPES) reaction buffer may lead to cleavage of AP sites in DNA via a β-elimination reaction (45), contributing to a false U-DNA incision activity. To investigate this possibility we compared hSMUG1 activity in HEPES and sodium cacodylate buffer in parallel experiments using otherwise identical conditions. The results showed no significant difference in incision activity between these two reaction buffers, which largely excludes possible artefacts related to reaction buffer composition (Figure 4F).

Sodium borohydride trapping experiments indicate no AP lyase function of hSMUG1

Because our results showed that hSMUG1 formed the same 3´-end products (3´-α,β-unsaturated aldehyde/UIP and 3´-phosphate/UPP) as certain bi-functional DNA glycosylases like hOGG1 and EcFpg, it was reasonable to investigate whether the enzyme execute catalysis by a similar lyase mechanism or function. Since the imine enzyme–DNA-deoxyribose (Schiff base) intermediate (34) of these glycosylases can be cross-linked to the DNA substrate (substrate 2) following treatment with sodium borohydride, which reduces the double bond of the complex, hSMUG1 reaction mixture was subjected to such treatment where EcFpg was assayed in parallel as a positive control. We performed such experiments with an enzyme concentration lower (Figure 6, left panel) as well as higher (Figure 6, right panel) than the substrate concentration using a 1 h incubation time. The results showed that like hUNG, which we used as a negative control, hSMUG1 did not form such a complex with U-DNA, arguing against the presence of a lyase active site amino residue in hSMUG1. This contrasted with the efficient trapping of AP-DNA as opposed to U-DNA by EcFpg, confirming the potency of the assay.

Indirect identification of UIP and UPP formed by hSMUG1 confirmed under conditions of no significant spontaneous AP-DNA incision

In addition to the indirect identification of UIP and UPP as incision products of hSMUG1 using sample-treatment with formamide at 95 °C (Figure 3A), the same result was obtained at conditions using no incubation nor exposure to higher temperature than 37 °C (Figure 7). In this case, hUNG rather than EcUng was employed converting U-DNA into AP-DNA while the same enzymes defined the different 3´-incision products, except that hAPE1 defined the 3´-OH and EcNth defined both the 3´-dRP as well as the corresponding 3´-α,β-unsaturated aldehyde (see *Comment on β-elimination products produced by EcNth and hOGG1* in Supplementary Data). The results showed that UIP (lane 7) migrates faster than the slowest migrating product defined by EcNth (*i.e.*, 3´-dRP; lane 5), slower than the 3´-OH product produced by hAPE1 (lane 4), and exactly like the fastest migrating 3´-incision product defined by EcNth (lane 5) and by hOGG1 (see Figure 3A, lane 5), which is the 3´-α,β-unsaturated aldehyde. The conversion of all substrate into product by incubation of hSMUG1 and EcFpg together (lane 6) verified that the hSMUG concentration employed was sufficient to remove all uracils from the DNA, as hUNG together with EcFpg, used as a control, also did (lane 3). A faint band corresponding to UPP, which migrated as the 3´-phosphate formed by EcFpg, was also observed (Figure 7). Consequently, the indirect identification of UIP and UPP without using heat treatment to denature DNA prior to analysis confirmed the previous identification (Figure 3A).

Chemical identification of UIP and UPP formed by hSMUG1 by MALDI-TOF-MS under conditions of no significant spontaneous AP-DNA incision

Although gel electrophoresis is a standard quantitative method for identification of BER cleavage-products, the identification is indirect and does not provide chemical parameters. For this reason, cleavage products of an un-labelled version of substrate 2 formed by hSMUG1 as well as enzymes used to define the different 3´-end products were further investigated using MALDI-TOF-MS analysis. We also performed incubations in solutions made in $H_2{}^{18}O$, to indicate reaction mechanism. Like hOGG1 but different from EcFpg and EcNfo (data not shown), hSMUG1 produced a 5´-DNA fragment of M/Z 3494.6, exactly corresponding to the mass of a fragment containing a 3´-α,β-unsaturated aldehyde (Figure 8A). Likewise, a signal of M/Z 3512.6 also appeared following enzyme digestion, even though enzyme reactions were carried out in $H_2{}^{18}O$ (Figure 8B, left). This indicates post-enzymatic addition of water (which mostly contains ^{16}O) to the 3´-α,β-unsaturated aldehyde, since such addition during enzyme reaction (mostly with ^{18}O) should result in a product of M/Z 3514.6 due to a 3´-^{18}OH group. When we precipitated the enzymatically exposed substrate with ethanol in the presence of ammonium acetate, the “M/Z 3512.6” product was absent. Instead, a signal corresponding to M/Z 3511.6 appeared, which can be explained by quantitative addition of ammonia to the double bond of the 3´-α,β-unsaturated aldehyde (Figure 8B, middle). When the reaction products were dissolved in $H_2{}^{18}O$ instead of normal water, the M/Z 3511.6 signal decreased in favour of a signal corresponding to M/Z 3513.6, which accord with the presence of an aldehyde group at C1´ (Figure 8B, right). Aldehydes are subject to exchange of oxygen isotopes by addition-elimination of

water. Thus, in addition to directly identifying a fragment with the same molecular weight as if it contains a 3´-α,β-unsaturated aldehyde (Figure 8A), the results also demonstrated two possible post-enzymatic derivatives of such a product (Figure 8B). This confirms the presence of a double bond and provides compelling evidence that the 5´ incision fragment formed by hSMUG1 is indeed a 3´-α,β-unsaturated aldehyde. MALDI-TOF-MS also showed that all incubations with hSMUG1, like all those with EcFpg (data not shown), produced a signal corresponding to M/Z 3396.6 (Figure 8A), exactly corresponding to the mass of a 5´-DNA fragment containing a 3´-phosphate. This provides compelling evidence that UPP formed by hSMUG1 (Figures 1B, 3A and 7), first identified by migrating as the β/δ-elimination product defined by EcFpg in PAGE (Figure 3A), is indeed a 3´-phosphate. We observed a signal with M/Z 4342.7 in all experiments, regardless whether or when we used ^{18}O- or ^{16}O-water or ammonium-based precipitation. This M/Z value corresponds to a 3´-fragment containing a 5´-phosphate end (Figure 8A). We did not observe any signal corresponding to a 5´-fragment containing a 3´-dUMP, which indicates that the formation of UIP follows uracil excision (Figure 8A). We also did not observe any signal corresponding to the masses of UIP or other possible U-DNA incision or processing products in control incubation without repair enzyme (Supplementary Data, Figure S3). Finally, we observed a signal of M/Z 3316.5 corresponding to a 3´-OH when substrate subjected to hSMUG1 was further incubated with hAPE1 (Supplementary Data, Figure S4), as previously demonstrated by PAGE (Supplementary Data, Figure S1).

Kinetic model

To describe hSMUG1 excision and incision activity we compared and adapted the experimental data to a three-phase kinetic model (Figure 9A; see Materials and Methods and Supplementary Data), which agrees well with the measured U-DNA incision and uracil excision rate (Figures 9B and 9C, respectively). Phase 1 involves an initial rapid recognition and excision of uracil to form AP-DNA (Figure 9A, upper and lower panels). Phase 2 is a slower adsorption/desorption phase where hSMUG1 (E) binds non-specifically at different sites on DNA establishing a dynamic equilibrium (steady state) including the AP site to be cleaved. Phase 3 includes the incision of the AP site and depends on the enzyme concentration. While the rapid increase in incision velocity occurring at low initial concentrations (Figure 9B) can be explained by rapid rebinding to AP site after uracil excision (Figures 9A and 9B, low $[E]_0$), the much slower increase in incision rate at high initial concentrations (Figures 9A and 9B, high $[E]_0$) now depends on the bulk (free in solution) enzyme concentration and follows Michaelis-Menten kinetics (V^{in} becomes now linearly dependent with respect to $[E]_0$, Figure 9B), because only binding to the AP site causes incision. In agreement with the assumption that excision is a rapid process the excision rate V^{ex} follows Michaelis-Menten kinetics as seen experimentally (Figure 9C). Figures 9D and 9E show concentration time plots for incision product P1 and excision product U when initial substrate concentration is 50 nM and the initial enzyme concentration varies in the range 0.05 nm to 0.25 nM. It is seen that during the 20 min incubation time most of the substrate S is transformed into excision products, while only a fraction of S forms incision products. The model resulted in a K_D of 0.0001 nM, a k_P^{ex} of 200 min^{-1} for uracil excision and a k_2^{in} of 0.2 min^{-1} for U-DNA incision (Table 1; see *A three-phase kinetic model* in Supplementary Data). Also,

for higher initial DNA concentration (125 and 375 nM) a good agreement between experimental and model data was found (Supplementary Data, Figures S5A and S5B, respectively).

DISCUSSION

In the present study we demonstrate, that the family 3 UDG hSMUG1–hitherto regarded as a mono-functional DNA glycosylase–incises the phosphodiester backbone of U-DNA at the lesion site after uracil has been excised (Figures 1B and 4B). The activity is dependent on that the uracil base itself is recognised by the enzyme, since no significant activity was detected on AP site-containing DNA (data not shown), which encouraged us to call the 3´-incision product UIP. Judged from migration behaviour in gel electrophoresis hSMUG1 seemed to form the same 5´-fragment as the major fragment formed by hOGG1 (Figure 3A) as well as one of the fragments produced by EcNth (Figure 7; see *Comment on β-elimination products produced by EcNth and hOGG1* in Supplementary Data). This ends with a 3´-α,β-unsaturated aldehyde (Figure 7), and is exactly the same product as formed by thermolysis of AP-DNA at neutral pH (Figure 2B) (39). In addition to UIP, which is the major product formed by hSMUG1, the enzyme also forms a minor product (Figure 1B), which becomes a major product, following extended incubation times (Figure 3A), which we decided to call UPP. UPP migrated in PAGE as the β/δ-elimination product formed by EcFpg (Figures 1B and 3A).

Subsequent MALDI-TOF-MS analyses of hSMUG1-exposed U-DNA using the same 3´-end-defining enzymes as positive controls confirmed the indirect identification by PAGE of both UIP and UPP. Thus, the molecular mass of UIP corresponded exactly to the presence of a 3´-α,β-unsaturated aldehyde, while the molecular mass of UPP was identical to the mass of a 3´-phosphate (Figure 8A). Both UIP and UPP are known products of bi-functional DNA glycosylases shown to be processed *in vitro* to 3´-OH by hAPE1 (Supplementary Data, Figures S1 and S5) and hPNKP, respectively (29), which suggest efficient downstream processing *in vivo* by priming the nick for deoxycytidine monophosphate (dCMP) insertion and ligation (Figure 10).

Opposed to the ability of the gel analysis, the MALDI-TOF-MS results also showed the presence of a 5´-phosphate on the 3´-fragment completing the analysis of the hSMUG1-processed U-DNA (Figure 8A). Enzyme reactions performed in the presence $H_2{}^{16}O$ and $H_2{}^{18}O$ (Figure 8B) were consistent with a β-elimination reaction mechanism. However, the failure to trap a UDG–DNA reaction intermediate as a stable covalent complex (Figure 6) and the fact that hSMUG1 lacks an active site lysine (15,18,46) to carry out a β- or a β/δ-elimination reaction indicates that the excision and incision activities are not concerted. We propose that incision occurs in two steps. In the first step, the cleavage of the N-glycosidic bond may be similar to the SN1-like mechanism of hUNG (47,48), where stereo-electronic effects lead to the formation of a uracil anion and an AP site with a positively charged C1´. In the second step, a β-elimination reaction can occur by deprotonation of the deoxyribose C2´ and the formation of an enolate intermediate at the formyl group (Figure 8A).

However, the general base necessary for the C2´ deprotonation as well as a way to stabilise the enolate intermediate need to be specified.

The crystal structure of *Xenopus laevis* SMUG1 (xSMUG1) has been determined and together with its amino acid sequence compared to other members of the UDG superfamily (15,18,46). Human and amphibian SMUGs share high level of sequence similarity in the catalytic active site. Since hSMUG1 has not been crystallised together with substrate, its similar organisation of the active site as other members of the UDG superfamily like the much studied hUNG suggests comparisons with the latter, especially hUNG crystals with substrate (14,49). One of the original models for catalysis by family 1 UDGs suggested an associative SN2 mechanism, which shortly says that following flipping into the active site uracil is released from deoxyribose by attack on the C1´ of a water molecule activated by an Asp residue acting as a general base (Asp145 in hUNG, with possible assistance from His148) (14,31,50). In contrast, later results supported by biophysical investigations have favoured a dissociative SN1-like mechanism, which means that following base flipping into the active site the glycosidic bond splits into a uracil anion stabilised by a histidine residue and a deoxyribose oxocarbenium ion (47). Then, a water molecule, coordinated by certain active site amino acid residues, somewhat passively becomes the 1´-α-OH C1´ after dissociation of the uracil anion (47). While the SN2 approach focuses on the activation of a H_2O nucleophile by certain amino acid residues (14), the SN1 model emphasises the reaction energy contributed by molecular strain or other unfavourable atomic clashes in U-DNA before and following base flipping (49). Because hSMUG1 contains the nonpolar Asn85 unable to activate H_2O (for nucleophilic attack or elimination) in place of the activating Asp145 of hUNG (48), the SN1-like mechanism might appear applicable for hSMUG1 as well (46). That may explain the observation that the U-DNA excision activity of hUNG is more effected by replacement of Asp145 than the activity of hSMUG1 is effected by replacement of Asn85 (18,46). If we, being conscious about our limitations at the present stage of knowledge, assume a similar SN1-like reaction intermediate for hSMUG1 as shown for hUNG, Asn85 of hSMUG1 can be assigned to coordinate the reactive water molecule to attach the deoxyribose oxocarbenium ion, and that the events occurs in a non-concerted manner via the activation of the uracil anion. In the crystal structure of xSMUG bound to free uracil, the backbone carbonyl group of Asn96 (corresponds to Asn85 of hSMUG1) coordinates water by a hydrogen bond (Figure 8A).

A β-elimination reaction at the C2´–C3´ bond accords with the direct formation of UIP from the abasic sugar. Since the trapping experiment indicated no formation of an imine intermediate (Figure 6), theoretically, the elimination reaction may occur via deprotonation of C2´ leading to formation of the enolate intermediate (Figure 8A), although the O1´ negative charge may require stabilisation. However, in the case of hUNG which also was crystallised together with AP-DNA (51), attachment to the AP site compresses, like ordinary unspecific DNA binding, the DNA backbone to promote nucleotide flipping. Since hSMUG1 binds AP sites much stronger than hUNG (18), such induced strain may contribute to reaction energy. A major limitation of the model is our inability to specifically suggest certain active site residues as *e.g.* the deprotonating general base and/or the enolate stabiliser, which will require a much more detailed molecular understanding of the interactions of

hSMUG1 with AP-DNA than presently available. In the case of UPP, it should be realised that the present data does not clarify whether it is formed directly through strand incision or by processing of UIP (Figure 8A), pointing to an uncertainty of the reaction mechanism not yet settled.

We developed a three-phase kinetic model which predicts rapid uracil excision in phase 1, slow unspecific enzyme adsorption/desorption to DNA in phase 2 and enzyme-dependent AP site incision in phase 3 (Figure 9A). This working model is the result of (failed) attempts to view/model the experimental data by simpler models. Although, in principle, other mechanisms cannot be ruled out, we arrived at the three stage model because non-specific binding of the enzyme on the substrate DNA appears necessary to describe the observed transition of the U-DNA incision rate (V^{in}) from rapid kinetics (low $[E]_0$) to a less rapid increase at higher $[E]_0$ values (Fig. 9C).

Recently it was discovered that hSMUG1 probably is involved in RNA quality control *in vivo*. Cellular depletion of the enzyme caused accumulation of 5-hydroxymethyluridine in rRNA, and hSMUG1 exhibited activity for 5-hydroxymethyldeoxyuridine, but not uracil, in a single-stranded RNA context *in vitro* (52). This revelation of the absence of a direct overlap between the DNA and RNA substrates adds to the complexity of substrate recognition and binding by hSMUG1, which together with the different catalytic potentials described here suggest studies on how hSMUG1 interacts and reacts with altered bases in DNA and RNA in parallel.

We conclude that the BER pathway is more dynamic than previously anticipated after showing that hSMUG1 may execute a second incision step following base excision resulting in very toxic strand breaks and blocked 3´-ends, with delayed AP endonuclease-mediated processing *in vivo* as a consequence (Figure 10). The finding that human poly(ADP-ribose) polymerase-1 efficiently binds AP sites and also exhibits AP lyase activity may serve a similar function (53). It is tempting to speculate whether this might be an advantageous alternative under certain cellular stress conditions, to delay the initiation of repair replication. During circumstances of large base damage load, it might be crucial to decrease the number of replication forks to minimize the possibility for genomic collapse. Our findings contribute to the emerging knowledge on how BER is intricately carried out at many levels (54,55). It has also been reported that hAPE1 has a high affinity for and is able to incise–although at an extremely low rate–U-DNA, leaving behind a 5′-terminal dUMP (56). This adds to the dynamic and complexity of U-DNA repair. Since the relative importance of the AP lyase, AP endonuclease and PNKP functions in BER has been much discussed, and may vary in different species, more studies are needed to establish their roles *in vivo* and from now also their roles compared to the novel U-DNA incision activity presented here. Lastly we suggest that this activity also may represent a hAPE1-independent nicking of the DNA as a part of the mechanism involved in class-switch recombination and somatic hyper-mutation (21).

SUPPLEMENTARY DATA

Supplementary Data are available at NAR online.

FUNDING

This research was supported by University of Stavanger and Oslo University Hospital/University of Oslo.

CONFLICT OF INTEREST

None declared.

ACKNOWLEDGEMENT

We thank E.C. Ludvigsen and M. Høie for technical assistance, and K. H. Hopmann and K.B. Jørgensen for discussions on enzyme and organic reaction mechanism.

REFERENCES

1. Lindahl, T. (1993) Instability and decay of the primary structure of DNA. *Nature*, **362**, 709–715.
2. Friedberg, E.C., Walker, G.C., Siede, W., Wood, R.D., Schultz, R.A. and Ellenberger, T. (2006) *DNA Repair and Mutagenesis*. 2nd ed. ASM Press, Washington, DC.
3. Alexandrov, L.B., Nik-Zainal, S., Wedge, D.C., Aparicio, S.A., Behjati, S., Biankin, A.V., Bignell, G.R., Bolli, N., Borg, A., Børresen-Dale, A.L. *et al.* (2013) Signatures of mutational processes in human cancer. *Nature*, **500**, 415–421.
4. Kornberg, A. and Baker, T.A. (1992) *DNA Replication*. 2nd ed. W.H. Freeman, New York.
5. Bauer, N.C., Corbett, A.H. and Doetsch, P.W. (2015) The current state of eukaryotic DNA base damage and repair. *Nucleic Acids Res*, **43**, 10083–10101.
6. Kim, Y.-J. and Wilson, D.M., 3rd (2012) Overview of base excision repair biochemistry. *Curr Mol Pharmacol*, **5**, 3–13.
7. Pearl, L.H. (2000) Structure and function in the uracil-DNA glycosylase superfamily. *Mutat Res*, **460**, 165–181.
8. Haushalter, K.A., Todd Stukenberg, M.W., Kirschner, M.W. and Verdine, G.L. (1999) Identification of a new uracil-DNA glycosylase family by expression cloning using synthetic inhibitors. *Curr Biol*, **9**, 174–185.
9. Kavli, B., Sundheim, O., Akbari, M., Otterlei, M., Nilsen, H., Skorpen, F., Aas, P.A., Hagen, L., Krokan, H.E. and Slupphaug, G. (2002) hUNG2 is the major repair enzyme for removal of uracil from U:A matches, U:G mismatches, and U in single-stranded DNA, with hSMUG1 as a broad specificity backup. *J Biol Chem*, **277**, 39926–39936.
10. Bjelland, S. and Seeberg, E. (2003) Mutagenicity, toxicity and repair of DNA base damage induced by oxidation. *Mutat Res*, **531**, 37–80.
11. Boorstein, R.J., Cummings, A., Jr., Marenstein, D.R., Chan, M.K., Ma, Y., Neubert, T.A., Brown, S.M. and Teebor, G.W. (2001) Definitive identification of mammalian 5-hydroxymethyluracil DNA *N*-glycosylase activity as SMUG1. *J Biol Chem*, **276**, 41991–41997.
12. Masaoka, A., Matsubara, M., Hasegawa, R., Tanaka, T., Kurisu, S., Terato, H., Ohyama, Y., Karino, N., Matsuda, A. and Ide, H. (2003) Mammalian 5-formyluracil-DNA glycosylase. 2. Role of SMUG1 uracil-DNA glycosylase in repair of 5-formyluracil and other oxidized and deaminated base lesions. *Biochemistry*, **42**, 5003–5012.
13. Darwanto, A., Theruvathu, J.A., Sowers, J.L., Rogstad, D.K., Pascal, T., Goddard, W., 3rd and Sowers, L.C. (2009) Mechanisms of base selection by human single-stranded selective monofunctional uracil-DNA glycosylase. *J Biol Chem*, **284**, 15835–15846.
14. Slupphaug, G., Mol, C.D., Kavli, B., Arvai, A.S., Krokan, H.E. and Tainer, J.A. (1996) A nucleotide-flipping mechanism from the structure of human uracil-DNA glycosylase bound to DNA. *Nature*, **384**, 87–92.
15. Wibley, J.E.A., Waters, T.R., Haushalter, K., Verdine, G.L. and Pearl, L.H. (2003) Structure and specificity of the vertebrate anti-mutator uracil-DNA glycosylase SMUG1. *Mol Cell*, **11**, 1647–1659.
16. Nilsen, H., Haushalter, K.A., Robins, P., Barnes, D.E., Verdine, G.L. and Lindahl, T. (2001) Excision of deaminated cytosine from the vertebrate genome: role of the SMUG1 uracil-DNA glycosylase. *EMBO J*, **20**, 4278–4286.
17. Pettersen, H.S., Sundheim, O., Gilljam, K.M., Slupphaug, G., Krokan, H.E. and Kavli, B. (2007) Uracil-DNA glycosylases SMUG1 and UNG2 coordinate the initial steps of base excision repair by distinct mechanisms. *Nucleic Acids Res*, **35**, 3879–3892.
18. Pettersen, H.S., Sundheim, O., Gilljam, K.M., Slupphaug, G., Krokan, H.E. and Kavli, B. (2007) Uracil–DNA glycosylases SMUG1 and UNG2 coordinate the initial steps of base excision repair by distinct mechanisms. *Nucleic Acids Res*, **35**, 3879–3892.
19. Matsubara, M., Tanaka, T., Terato, H., Ohmae, E., Izumi, S., Katayanagi, K. and Ide, H. (2004) Mutational analysis of the damage-recognition and catalytic mechanism of human SMUG1 DNA glycosylase. *Nucleic Acids Res*, **32**, 5291–5302.
20. Krokan, H.E., Sætrom, P., Aas, P.A., Pettersen, H.S., Kavli, B. and Slupphaug, G. (2014) Error-free *versus* mutagenic processing of genomic uracil–relevance to cancer. *DNA Repair (Amst)*, **19**, 38–47.
21. Dingler, F.A., Kemmerich, K., Neuberger, M.S. and Rada, C. (2014) Uracil excision by endogenous SMUG1 glycosylase promotes efficient Ig class switching and impacts on A:T substitutions during somatic mutation. *Eur J Immunol*, **44**, 1925–1935.
22. Di Noia, J.M., Rada, C. and Neuberger, M.S. (2006) SMUG1 is able to excise uracil from immunoglobulin genes: insight into mutation versus repair. *EMBO J*, **25**, 585–595.

23. Maiti, A., Noon, M.S., MacKerell, A.D., Jr., Pozharski, E. and Drohat, A.C. (2012) Lesion processing by a repair enzyme is severely curtailed by residues needed to prevent aberrant activity on undamaged DNA. *Proc Natl Acad Sci USA*, **109**, 8091–8096.
24. Kohli, R.M. and Zhang, Y. (2013) TET enzymes, TDG and the dynamics of DNA demethylation. *Nature*, **502**, 472–479.
25. Weber, A.R., Krawczyk, C., Robertson, A.B., Kuśnierczyk, A., Vågbø, C.B., Schuermann, D., Klungland, A. and Schär, P. (2016) Biochemical reconstitution of TET1-TDG-BER-dependent active DNA demethylation reveals a highly coordinated mechanism. *Nat Commun*, **7**, 10806.
26. Doetsch, P.W. and Cunningham, R.P. (1990) The enzymology of apurinic/apyrimidinic endonucleases. *Mutat Res*, **236**, 173–201.
27. Mol, C.D., Izumi, T., Mitra, S. and Tainer, J.A. (2000) DNA-bound structures and mutants reveal abasic DNA binding by APE1 and DNA repair coordination [corrected]. *Nature*, **403**, 451–456.
28. Li, M. and Wilson, D.M., 3rd. (2014) Human apurinic/apyrimidinic endonuclease 1. *Antioxid Redox Signal*, **20**, 678–707.
29. Wiederhold, L., Leppard, J.B., Kedar, P., Karimi-Busheri, F., Rasouli-Nia, A., Weinfeld, M., Tomkinson, A.E., Izumi, T., Prasad, R., Wilson, S.H. *et al.* (2004) AP endonuclease-independent DNA base excision repair in human cells. *Mol Cell*, **15**, 209–220.
30. Beard, W.A. and Wilson, S.H. (2014) Structure and mechanism of DNA polymerase *β*. *Biochemistry*, **53**, 2768–2780.
31. Mol, C.D., Arvai, A.S., Slupphaug, G., Kavli, B., Alseth, I., Krokan, H.E. and Tainer, J.A. (1995) Crystal structure and mutational analysis of human uracil-DNA glycosylase: structural basis for specificity and catalysis. *Cell*, **80**, 869–878.
32. Leiros, I., Nabong, M.P., Grøsvik, K., Ringvoll, J., Haugland, G.T., Uldal, L., Reite, K., Olsbu, I.K., Knævelsrud, I., Moe, E. *et al.* (2007) Structural basis for enzymatic excision of N^1-methyladenine and N^3-methylcytosine from DNA. *EMBO J*, **26**, 2206–2217.
33. Bailly, V., Verly, W.G., O'Connor, T. and Laval, J. (1989) Mechanism of DNA strand nicking at apurinic/apyrimidinic sites by *Escherichia coli* [formamidopyrimidine]DNA glycosylase. *Biochem J*, **262**, 581–589.
34. Zharkov, D.O., Rieger, R.A., Iden, C.R. and Grollman, A.P. (1997) NH_2-terminal proline acts as a nucleophile in the glycosylase/AP-lyase reaction catalyzed by *Escherichia coli* formamidopyrimidine-DNA glycosylase (Fpg) protein. *J Biol Chem*, **272**, 5335–5341.
35. Douthwaite, S. and Kirpekar, F. (2007) Identifying modifications in RNA by MALDI mass spectrometry. *Methods Enzymol*, **425**, 3–20.
36. Radhakrishnan, K. and Hindmarsh, A.C. (1993) *Description and Use of LSODE*. National Aeronautics and Space Administration, Lawrence Livermore National Laboratory Report UCRL-ID-113855 Lewis Research Center, Cleveland, OH 44135-3191.
37. Bailly, V. and Verly, W.G. (1987) *Escherichia coli* endonuclease III is not an endonuclease but a β-elimination catalyst. *Biochem J*, **242**, 565–572.
38. Manoharan, M., Ransom, S.C., Mazumder, A., Gerlt, J.A., Wilde, J.A., Withka, J.A. and Bolton, P.H. (1988) The characterization of abasic sites in DNA heteroduplexes by site specific labeling with C-13. *J Am Chem Soc*, **110**, 1620–1622.
39. Sugiyama, H., Fujiwara, T., Ura, A., Tashiro, T., Yamamoto, K., Kawanishi, S. and Saito, I. (1994) Chemistry of thermal degradation of abasic sites in DNA. Mechanistic investigation on thermal DNA strand cleavage of alkylated DNA. *Chem Res Toxicol*, **7**, 673–683.
40. Mazumder, A., Gerlt, J.A., Absalon, M.J., Stubbe, J., Cunningham, R.P., Withka, J. and Bolton, P.H. (1991) Stereochemical studies of the *β*-elimination reactions at aldehydic abasic sites in DNA: endonuclease III from *Escherichia coli*, sodium hydroxide, and Lys-Trp-Lys. *Biochemistry*, **30**, 1119–1126.
41. Lindahl, T. and Andersson, A. (1972) Rate of chain breakage at apurinic sites in double-stranded deoxyribonucleic acid. *Biochemistry*, **11**, 3618–3623.
42. Darwanto, A., Farrel, A., Rogstad, D.K. and Sowers, L.C. (2009) Characterization of DNA glycosylase activity by matrix-assisted laser desorption/ionization time-of-flight mass spectrometry. *Anal Biochem*, **394**, 13–23.
43. Warner, H.R., Demple, B.F., Deutsch, W.A., Kane, C.M. and Linn, S. (1980) Apurinic/apyrimidinic endonucleases in repair of pyrimidine dimers and other lesions in DNA. *Proc Natl Acad Sci USA*, **77**, 4602–4606.
44. Boiteux, S., Coste, F. and Castaing, B. (2017) Repair of 8-oxo-7,8-dihydroguanine in prokaryotic and eukaryotic cells: Properties and biological roles of the Fpg and OGG1 DNA *N*-glycosylases. *Free Radic Biol Med*, **107**, 179–201.

45. Steullet, V., Edwards-Bennett, S. and Dixon, D.W. (1999) Cleavage of abasic sites in DNA by intercalator-amines. *Bioorg Med Chem*, **7**, 2531–2540.
46. Matsubara, M., Tanaka, T., Terato, H., Ohmae, E., Izumi, S., Katayanagi, K. and Ide, H. (2004) Mutational analysis of the damage-recognition and catalytic mechanism of human SMUG1 DNA glycosylase. *Nucleic Acids Res*, **32**, 5291–5302.
47. Dinner, A.R., Blackburn, G.M. and Karplus, M. (2001) Uracil-DNA glycosylase acts by substrate autocatalysis. *Nature*, **413**, 752–755.
48. Przybylski, J.L. and Wetmore, S.D. (2011) A QM/QM investigation of the hUNG2 reaction surface: the untold tale of a catalytic residue. *Biochemistry*, **50**, 4218–4227.
49. Parikh, S.S., Walcher, G., Jones, G.D., Slupphaug, G., Krokan, H.E., Blackburn, G.M. and Tainer, J.A. (2000) Uracil-DNA glycosylase–DNA substrate and product structures: Conformational strain promotes catalytic efficiency by coupled stereoelectronic effects. *Proc Natl Acad Sci USA*, **97**, 5083–5088.
50. Savva, R., McAuley-Hecht, K., Brown, T. and Pearl, L. (1995) The structural basis of specific base-excision repair by uracil-DNA glycosylase. *Nature*, **373**, 487–493.
51. Parikh, S.S., Mol, C.D., Slupphaug, G., Bharati, S., Krokan, H.E. and Tainer, J.A. (1998) Base excision repair initiation revealed by crystal structures and binding kinetics of human uracil-DNA glycosylase with DNA. *EMBO J*, **17**, 5214–5226.
52. Jobert, L., Skjeldam, H.K., Dalhus, B., Galashevskaya, A., Vågbø, C.B., Bjørås, M. and Nilsen, H. (2013) The human base excision repair enzyme SMUG1 directly interacts with DKC1 and contributes to RNA quality control. *Mol Cell*, **49**, 339–345.
53. Khodyreva, S.N., Prasad, R., Ilina, E.S., Sukhanova, M.V., Kutuzov, M.M., Liu, Y., Hou, E.W., Wilson, S.H. and Lavrik, O.I. (2010) Apurinic/apyrimidinic (AP) site recognition by the 5′-dRP/AP lyase in poly(ADP-ribose) polymerase-1 (PARP-1). *Proc Natl Acad Sci USA*, **107**, 22090–22095.
54. Parsons, J.L. and Dianov, G.L. (2013) Co-ordination of base excision repair and genome stability. *DNA Repair*, **12**, 326–333.
55. Prasad, R., Shock, D.D., Beard, W.A. and Wilson, S.H. (2010) Substrate channeling in mammalian base excision repair pathways: passing the baton. *J Biol Chem*, **285**, 40479–40488.
56. Prorok, P., Alili, D., Saint-Pierre, C., Gasparutto, D., Zharkov, D.O., Ishchenko, A.A., Tudek, B. and Saparbaev, M.K. (2013) Uracil in duplex DNA is a substrate for the nucleotide incision repair pathway in human cells. *Proc Natl Acad Sci USA*, **110**, E3695–E3703.

TABLE AND FIGURES LEGENDS

Table 1. Kinetic parameters of the U-DNA incision as compared to the uracil excision activity of hSMUG1

$[E]_0$ (nM)	$[S]_0$ (nM)	K_D (nM)	k_2^{in}; k_p^{ex} (min^{-1})
0.0035–7.5	50, 125, 375	0.0001	0.2
0.0035–7.5	50		200

U-DNA incision activity is in red; uracil excision activity is in blue. Kinetic constants were determined by "eye-balled" fit simulation of the adsorption isotherms of the saturation curves in $[E]_0$ (see Supplementary Data, *A three-phase kinetic model*, Equations 9 and 13; k_1 = 1.5 nM^{-1} min^{-1}, k_2 = 0.002 nM^{-1} min^{-1}) (36).

Figure 1. Indication of hSMUG1 incision at uracil in DNA. (**A**) DNA substrate and conventional base excision assay. (**B**, **C**) Protein dependence of U-DNA incision (red) and uracil excision (blue). hSMUG1 was incubated with U-DNA (substrate 1, 0.5 pmol) in 20 mM Tris-HCl, pH 8.0, 1 mM DTT, 1 mM EDTA, 70 mM KCl at 37 °C for 10 min. Each value in C represents the average (± SD) of three independent measurements. "U-DNA incision (total)" corresponds to the values obtained from measuring the strength of the bands on the gel in B (lanes 4–7); the "U-DNA incision (enzymatic)" values are calculated by subtracting the amount of AP site incision caused by the 5-min heat treatment at 95 °C (as presented in Figure 2D) from the "U-DNA incision (total)" values, where the number of AP sites formed by hSMUG1 equals the number of uracils excised as measured in parallel in B (lanes 6–10). Abbreviation: nt, nucleotides.

Figure 2. Thermolysis of AP-DNA at high temperature efficiently forms UIP as opposed to UPP. (**A**) DNA substrate (see below) and assay. (**B**) Time dependence for cleavage of AP-DNA at 95 °C. AP-DNA derived from substrate 1 (0.5 pmol) was treated with loading solution used in conventional denaturing PAGE [containing 80% (v/v) formamide]. UIP forms efficiently, while a smaller amount of UPP/δ-product appears at the longest incubation times. (**C**) Time dependence for cleavage of AP-DNA at different temperatures. AP-DNA derived from substrate 1 was used at 37 °C (1 pmol) and 95 °C (see B), while that used at 75 °C (1 pmol) was derived from substrate 2 (see Materials and Methods). Each value represents the average (± SD) of 6–15 (95 °C; red), 2–6 (75 °C; orange) or 5–6 (37 °C; dark grey) independent measurements. At 37 °C, PAGE was performed on a 15% (w/v) gel containing 3% (v/v) formamide, and identical experiments with AP-DNA dissolved in pure water also showed no significant DNA cleavage (data not shown). UPP (green) was only formed at 95 °C. (**D**) Time dependence for AP-DNA cleavage in different solutions at 95 °C. Treatment in loading solution (red; described in B), water (blue) or TE buffer (violet) showed that the initial cleavage of AP-DNA is virtually identical in the different aqueous solutions. To separate incised DNA from un-incised DNA the reaction products were subjected to denaturing (red) or non-denaturing (blue; violet) PAGE. Each value represents the average (± SD) of 4–17 independent measurements, where the slopes of the graphs for the initial DNA incision, *i.e.* the first three data points (6–17 independent measurements; red, y = 3.95x + 0.769, R = 0.999; blue, y = 3.92x + 9.29, R = 0.998; violet, y = 3.65x + 27.673, R = 0.999) yield the non-enzymatic incision per min. This amounted to 3.95% of the AP sites incised per min, resulting in a background of 19.8% non-enzymatic hydrolysis (as calculated from the red graph; for the 5 min formamide/heat treatment) for the experiment described in Figures 1B and 1C. The amount of background incision was subtracted giving the value for enzymatic U-DNA incision for all experiments using 5 min heat treatment at 95 °C (Figure 1C). (**E**) Time dependence for AP-DNA cleavage in different solutions at 75 °C. AP-DNA (substrate 2, 1 pmol) was exposed to loading solution (red) or water (blue). Each value represents the average (± SD) of 6 (at 2–20 min) or 2–3 (at 30 min) independent measurements. To separate incised DNA from un-incised DNA the reaction products were subjected to denaturing (red) or non-denaturing (blue) PAGE. The initial slopes of the graphs (red, y = 0.722x + 3.65, R = 0.986; blue, y = 0.755x + 7.68, R = 0.977) yield the non-enzymatic

incision per min. This amounted to 0.722% of the AP sites incised per min in the formamide solution. Abbreviation: δ, β/δ-elimination product.

Figure 3. Indirect identification of UIP and UPP by electrophoretic mobility using conventional denaturing conditions. (**A**, **B**) Time dependence of UIP (red) and UPP (green) formation by hSMUG1. hSMUG1 (0.3 pmol) was incubated with substrate 1[^{32}P] (0.12 pmol) in 20 mM Tris-HCl, pH 8.0, 1 mM DTT, 1 mM EDTA, 70 mM KCl at 37 °C. To define the different 3´-end products, substrate was incubated with either EcNth (8.7 pmol), EcNfo (0.16 pmol), EcFpg (17 pmol) or hOGG1 (13 pmol) together with EcUng (0.78 pmol) for 10 min. Incised was separated from un-incised DNA by denaturing PAGE. Each value in B represents the average (± SD) of 3 independent measurements.

Figure 4. hSMUG1 incises at uracil in DNA. (**A**) DNA substrate and assay. (**B**, **C**) Protein dependence of U-DNA incision (red) and uracil excision (blue). hSMUG1 was incubated with U-DNA (substrate 1, 1 pmol) at 37 °C for 10 min. Each value in C represents the average (± SD) of 3–6 independent measurements. Incision product was separated from un-incised DNA by PAGE at 115 V for 1.5 h using a 20% (w/v) gel with 3% (v/v) formamide. (**D**) hSMUG1(25–270) was incubated with U-DNA (1 pmol of substrate 1; see A) at 37 °C for 20 min. Incision product was separated from un-incised DNA by PAGE at 120 V for 2 h using a 20% (w/v) gel with 3% (v/v) formamide. (**E**) Protein dependence of U-DNA incision/processing (red) and uracil excision (blue). Each value represents the average (± SD) of 4–5 independent measurements as described in D. (**F**) U-DNA incision by hSMUG1 in different buffers. U-DNA (1 pmol of substrate 1) was incubated with 1 pmol of hSMUG1(25–270) or without enzyme as control in reaction buffer (HEPES), or in 45 mM sodium cacodylate with the same pH and additions as for reaction buffer (see Materials and Methods), at 37 °C for 10 min (final volume, 20 µl). Incision product was separated from un-incised DNA by PAGE as described in E. Each value represents the average (± SD) of 3 independent measurements.

Figure 5. hSMUG1 incises at uracil in ssDNA. (**A**, **B**) Protein dependence of U-DNA incision (red) and uracil excision (blue). hSMUG1 was incubated with ssU-DNA (1 pmol; the labelled strand of substrate 1) at 37 °C for 10 min. Each value in B represents the average of 2 independent measurements. Incision product was separated from un-incised DNA by PAGE at 100 V for 50 min using a 12% (w/v) gel with 3% (v/v) formamide.

Figure 6. Trapping experiments for Schiff base intermediate. Left panel, EcFpg (17 pmol) alone as a negative control, and together with EcUng (3 pmol) as a positive control, EcUng as well as hUNG (5 pmol) alone as negative controls, and hSMUG1 (0.3 pmol) alone, were incubated with substrate 2 (1 pmol) and 50 mM $NaBH_4$ in reaction buffer at 37 °C for 1 h (final volume, 10 µl). Right panel, EcFpg (10 pmol) alone as a negative control, and together with EcUng (10 pmol) as a positive control, EcUng as well as hUNG (10 pmol) alone as negative controls, and hSMUG1 (10 pmol) alone, were incubated with substrate 2 (1 pmol) and 50 mM $NaBH_4$ in reaction buffer at 37 °C for 1 h (final volume, 10 µl). In each case (A and B), trapped was separated from un-trapped substrate by denaturing PAGE [10% (w/v)] at 200 V for 1 h. The experiments were performed in triplicate showing the same result.

Figure 7. Indirect identification of UIP by electrophoretic mobility without exposure of DNA to high temperature. U-DNA (substrate 1, 1 pmol) was incubated with hSMUG1 (0.3 pmol) at 37 °C for 30 min; either alone or together with EcFpg (4 pmol) as indicated. To define the different 3´-end products, substrate was incubated with hUNG (1 pmol) together with either EcFpg (4 pmol), hAPE1 (0.45 pmol) or EcNth (1 pmol), as indicated, under the same conditions. Incubations were also performed with either substrate 1 (dsDNA; lane 2) or the labelled strand of substrate 1 (ssDNA; lane 1) alone, showing that the upper substrate band is ssDNA and the lower band dsDNA. Incision product was separated from un-incised DNA by PAGE at 300 V for 5 h using a 20% (w/v) gel with 7 M urea.

Figure 8. Chemical identification of UIP and UPP and working model for reaction mechanism causing DNA incision. (**A**) Proposed E2 elimination reaction for the formation of UIP and chemical identification of UIP and UPP by MALDI-TOF-MS (see Supplementary Data, Figure S3 for MALDI-TOF-MS controls). hSMUG1 amino acid residue(s) suggested being involved in catalysis are coloured green; their hydrogen bonds with catalytic water and substrate are shown by red dotted lines. Proposed electronic and proton transfers involved in the formation of UIP are indicated by blue arrows. In the case of UPP, no reaction mechanism is proposed, and it is still unclear whether it is formed directly as a result of incision or by processing of UIP as depicted here. (**B**) Confirmation of the chemical nature of UIP. The observed post-enzymatic addition of water (left) or ammonia (middle and right) can be explained by the presence of a conjugated double bond, while the efficient exchange of an oxygen atom when the sample was transferred between ^{18}O- and ^{16}O-water can be explained by the presence of an aldehyde group. The MALDI-TOF-MS signals of the different chemical structures are shown in the upper and lower panels in A, and in the lower panel in B.

Figure 9. hSMUG1 kinetics. (**A**) Three-phase kinetic model. Phase 1 is shown in blue, phase 2 in violet and phase 3 in red. The uracil excision step is rapid compared to the slow DNA incision step. (**B**) U-DNA incision rate V^{in} and (**C**) uracil excision rate V^{ex} (see A) as a function of enzyme concentration $[E]_0$ at an initial U-DNA concentration $[S]_0$ of 50 nM, where the corresponding time-dependent data in the range $[E]_0$ = 0.05–0.25 nM (red line) is presented in (**D**) showing that at higher initial enzyme (E) concentration the model predicts that the formation of the incision product P1 has linear time-dependent kinetics, and in (**E**), showing that the excision kinetics for U (blue line) are fast and correlate with the removal of substrate DNA (S; black line), respectively. Incubation was performed for 20 min as described in Figure 4B. The V^{in} in the blue area changes as a result of increased unspecific binding of enzyme to DNA. In the yellow area, the unspecific binding is saturated and the V^{in} follows Michaelis-Menten (MM) kinetics. Each value represents the average (± SD) of 3–6 independent measurements. (**D**)

Figure 10. Proposed steps in the human BER pathway after SMUG1 has targeted uracil in DNA. After uracil has been removed by the DNA glycosylase activity of SMUG1 (step 1; blue), the latter is either replaced by APE1 (dark red) which incises the AP site (step 2a), or SMUG1 itself incises the AP site (step 2b; red) leaving behind a 3´-α,β-unsaturated aldehyde (UIP) which can be removed by APE1 (step 3b). Further processing of UIP (or maybe an alternative type of incision of the AP site;

green broken arrows) results in a 3´-phosphate (UPP) which is a substrate for PNKP (orange). The cleaned one nucleotide gap in DNA is now ready for insertion of the correct dCMP (step 4) by the repair DNA polymerase β (Pol β; dark blue), which also exhibits the dRP lyase activity which removes the 5´-dRP remnant (step 3a) after APE1 incision. BER is concluded by nick-sealing (step 5) by DNA ligase III (LIG3; purple). The residues removed are indicated in dark red; those resulting from replacement in dark blue, respectively; dR, deoxyribose.

A

Fig. 1

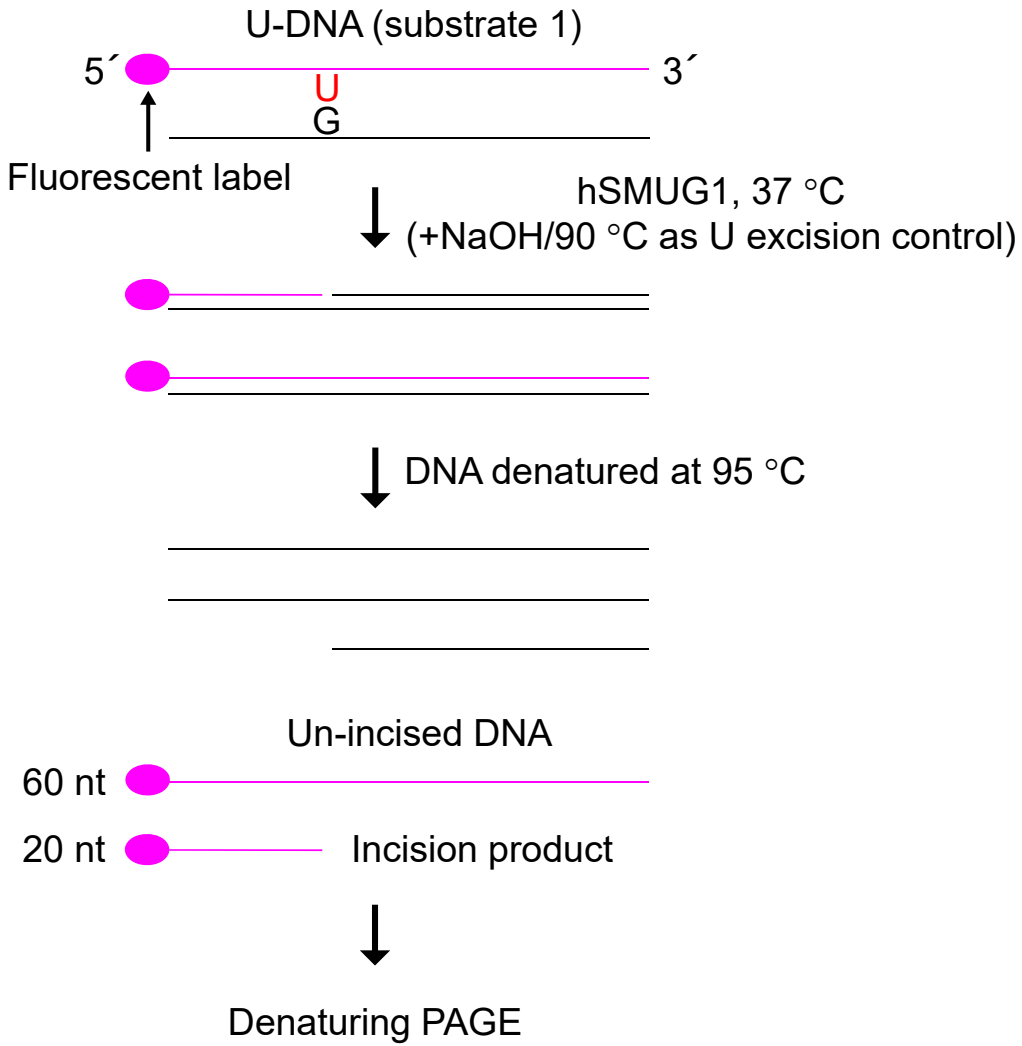
U-DNA (substrate 1)
5´
3´
U
G
Fluorescent label
hSMUG1, 37 °C
(+NaOH/90 °C as U excision control)
DNA denatured at 95 °C
Un-incised DNA
60 nt
20 nt
Incision product
Denaturing PAGE

B

Fig. 1

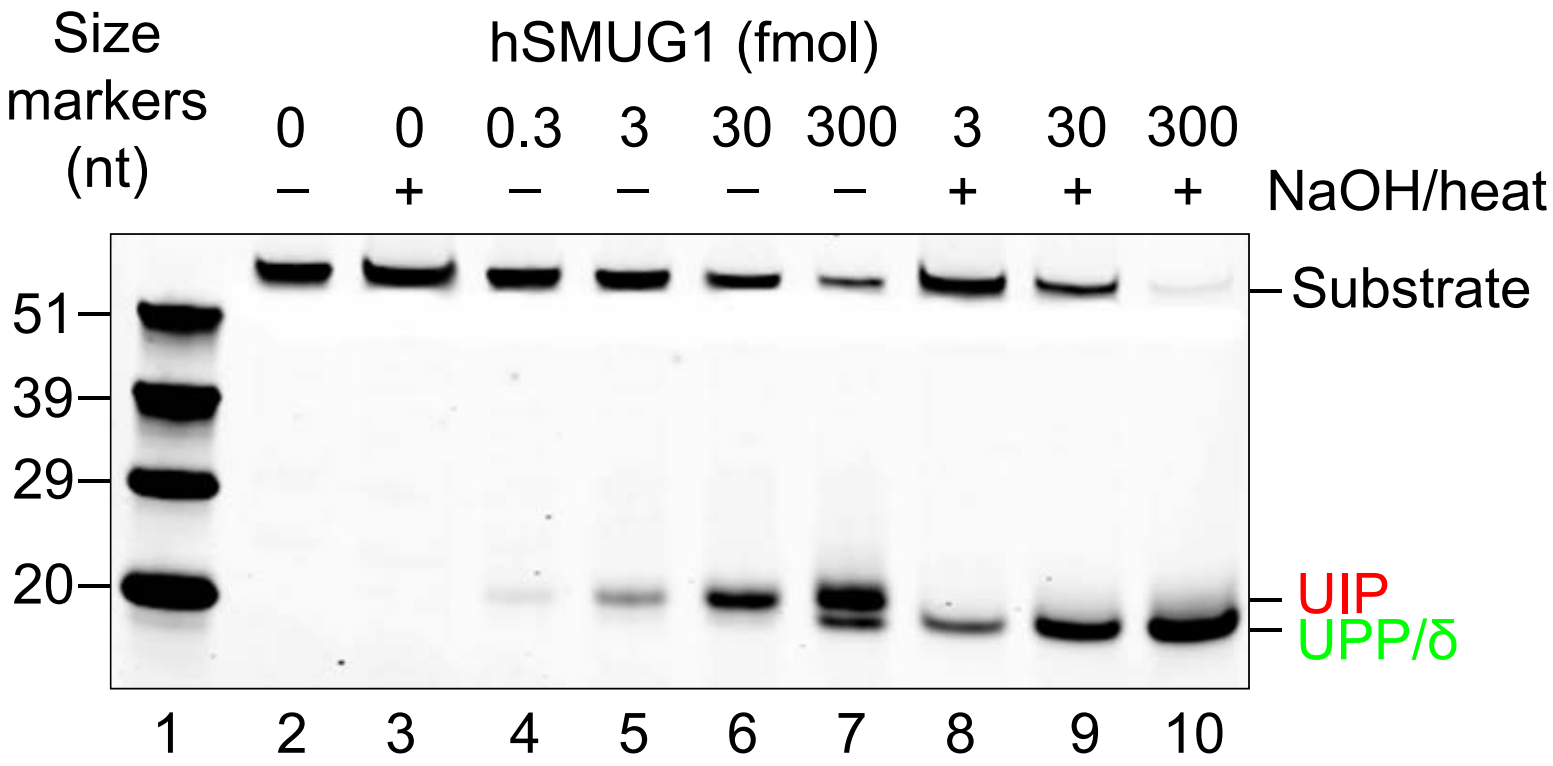
Size markers (nt)
hSMUG1 (fmol)
0 0 0.3 3 30 300 3 30 300
– + – – – – + + +
NaOH/heat
51
39
29
20
Substrate
UIP
UPP/δ
1 2 3 4 5 6 7 8 9 10

C

Fig. 1

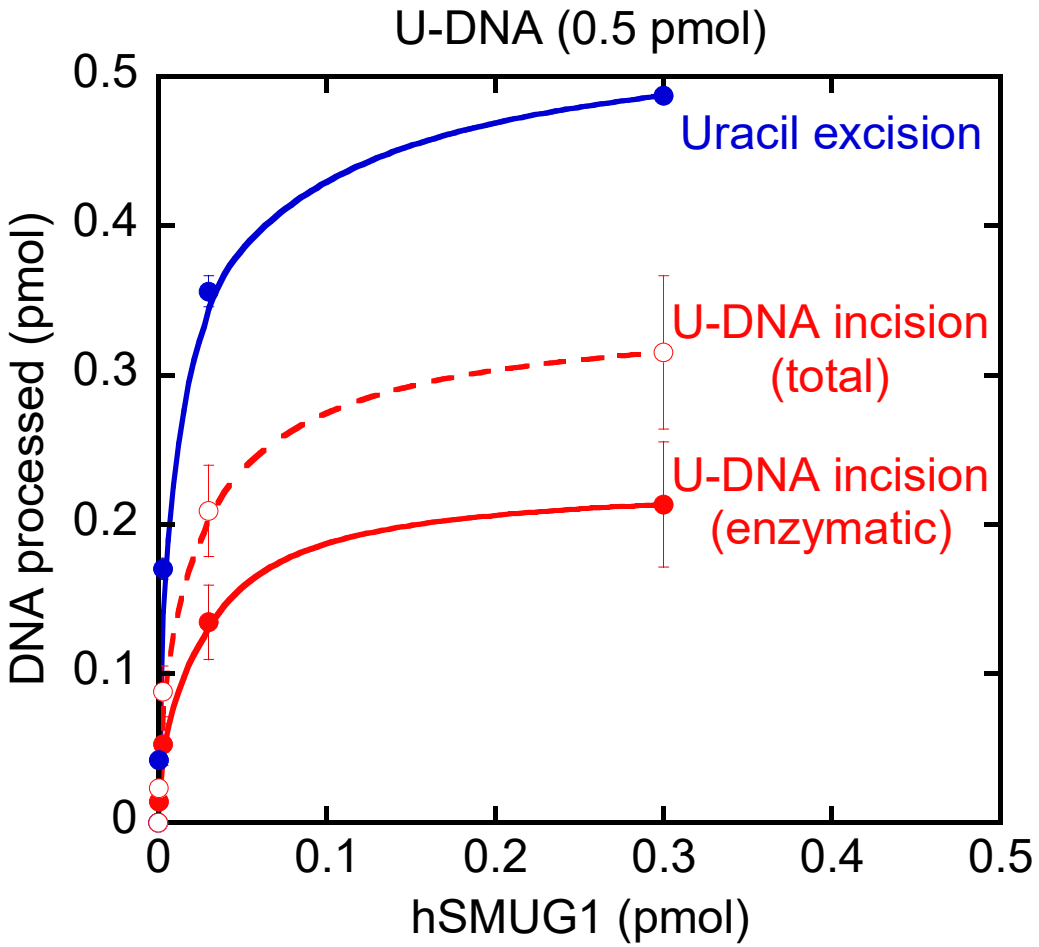
U-DNA (0.5 pmol)
DNA processed (pmol)
hSMUG1 (pmol)
0
0.1
0.2
0.3
0.4
0.5
Uracil excision
U-DNA incision
(total)
U-DNA incision
(enzymatic)

Fig. 2

A

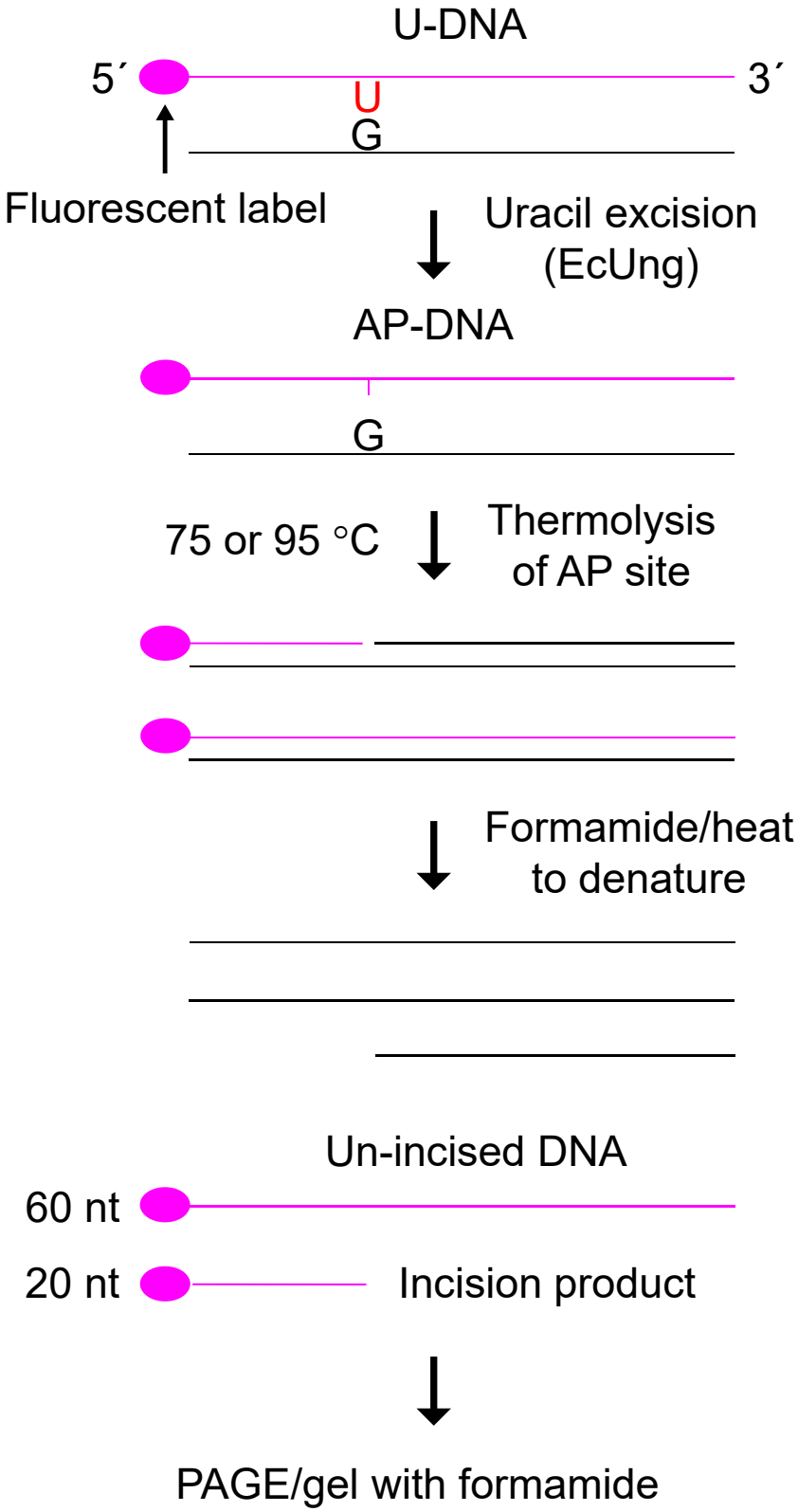
U-DNA
5´
3´
U
G
Fluorescent label
Uracil excision
(EcUng)
AP-DNA
G
75 or 95 °C
Thermolysis
of AP site
Formamide/heat
to denature
Un-incised DNA
60 nt
20 nt
Incision product
PAGE/gel with formamide

Fig. 2

B

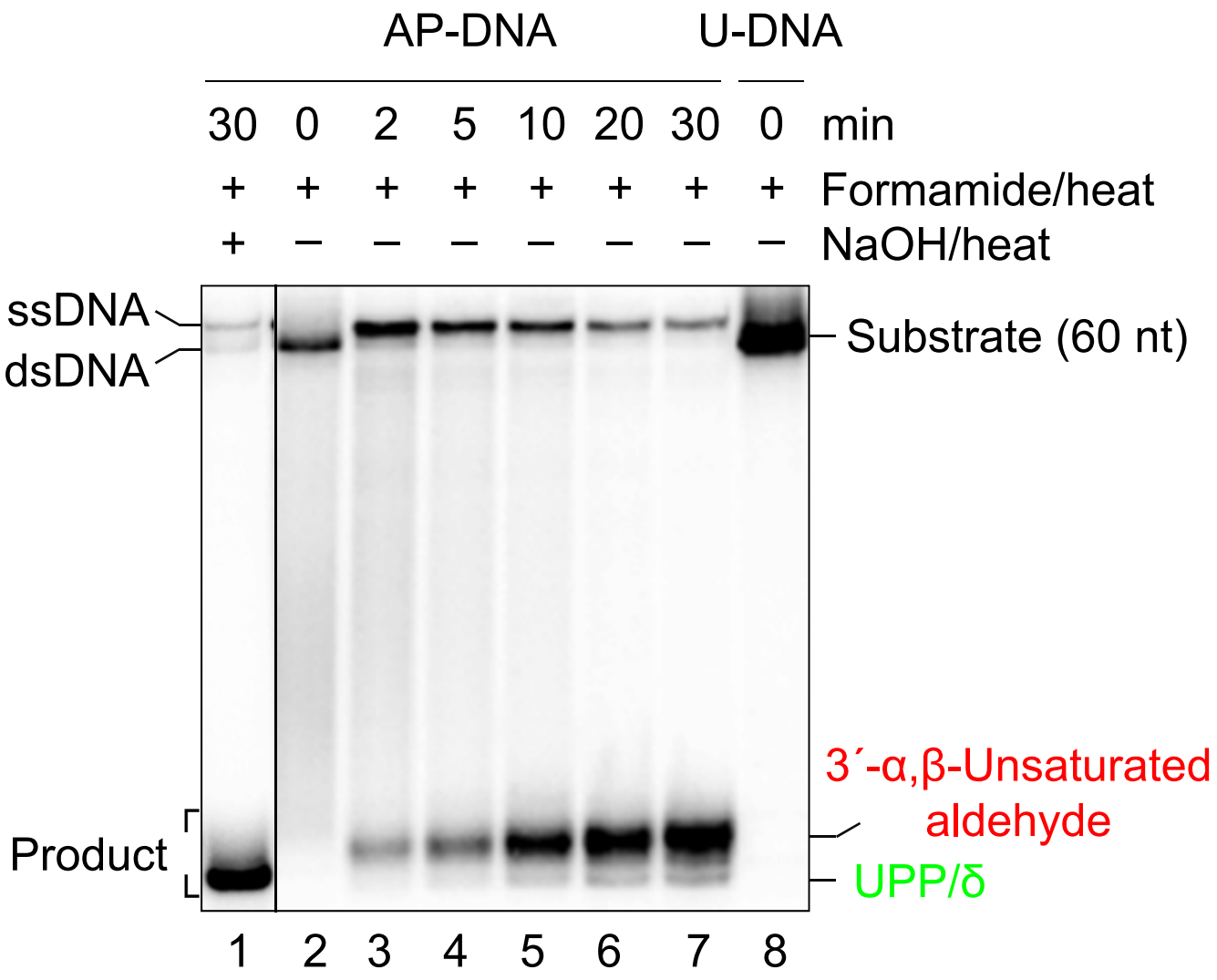
AP-DNA
U-DNA
30 0 2 5 10 20 30 0 min
+ + + + + + + + Formamide/heat
+ – – – – – – – NaOH/heat
ssDNA
dsDNA
Substrate (60 nt)
3´-α,β-Unsaturated aldehyde
Product
UPP/δ
1 2 3 4 5 6 7 8

Fig. 2

C

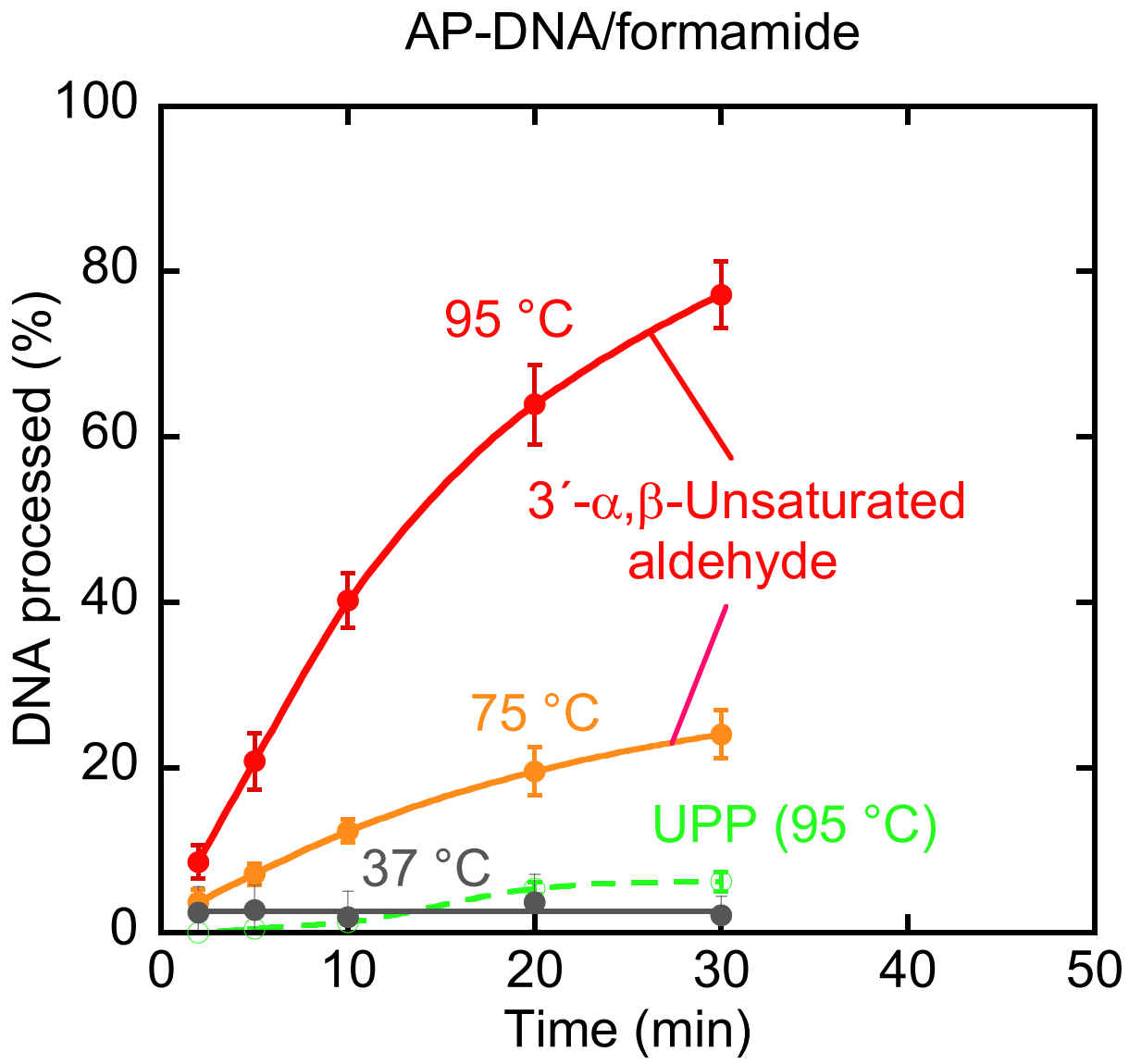
AP-DNA/formamide
DNA processed (%)
100
80
60
40
20
0
0
10
20
30
40
50
Time (min)
95 °C
3´-α,β-Unsaturated
aldehyde
75 °C
UPP (95 °C)
37 °C

Fig. 2

D

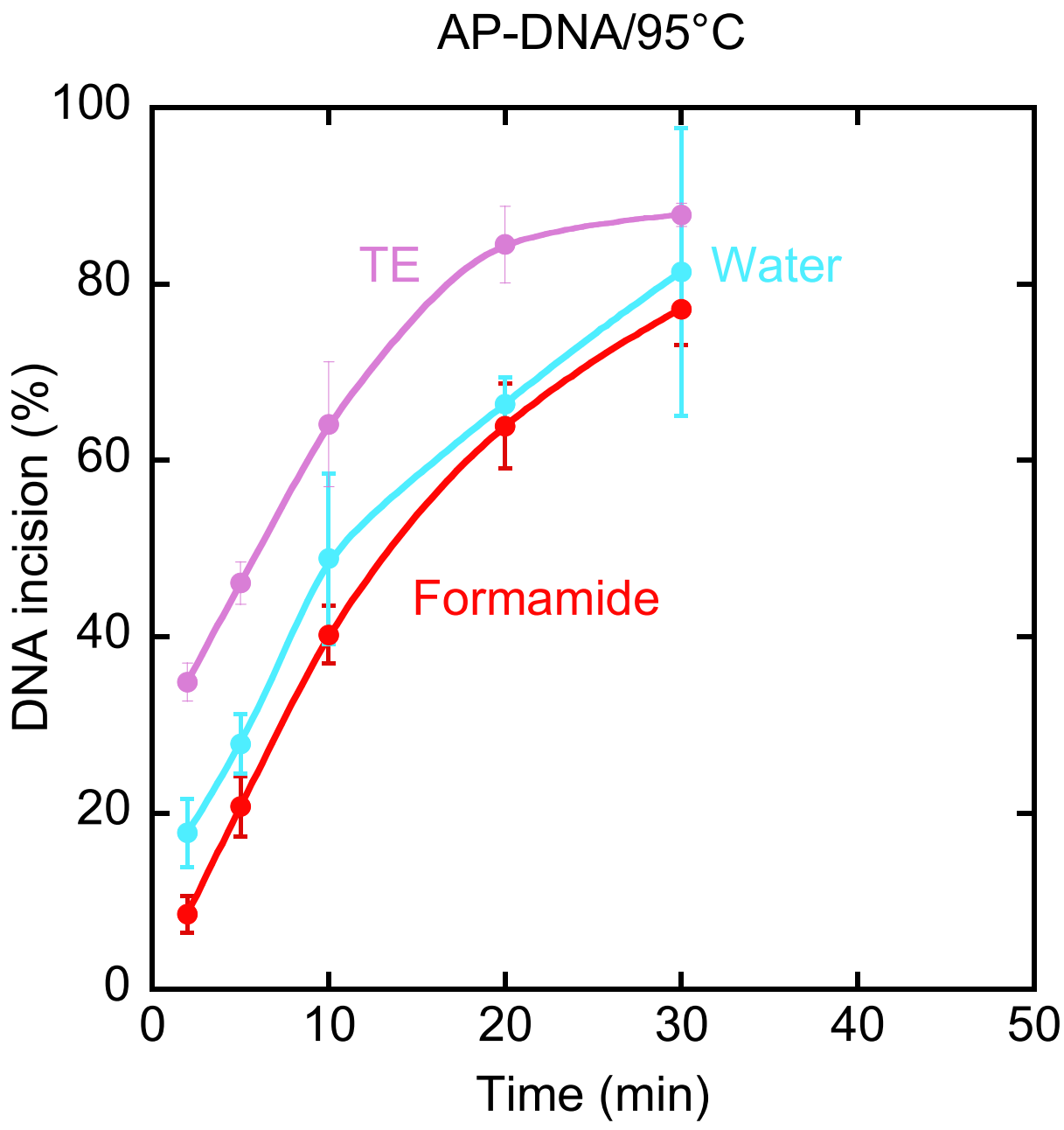
AP-DNA/95°C
DNA incision (%)
Time (min)
TE
Water
Formamide
0
20
40
60
80
100
0
10
20
30
40
50

Fig. 2

E

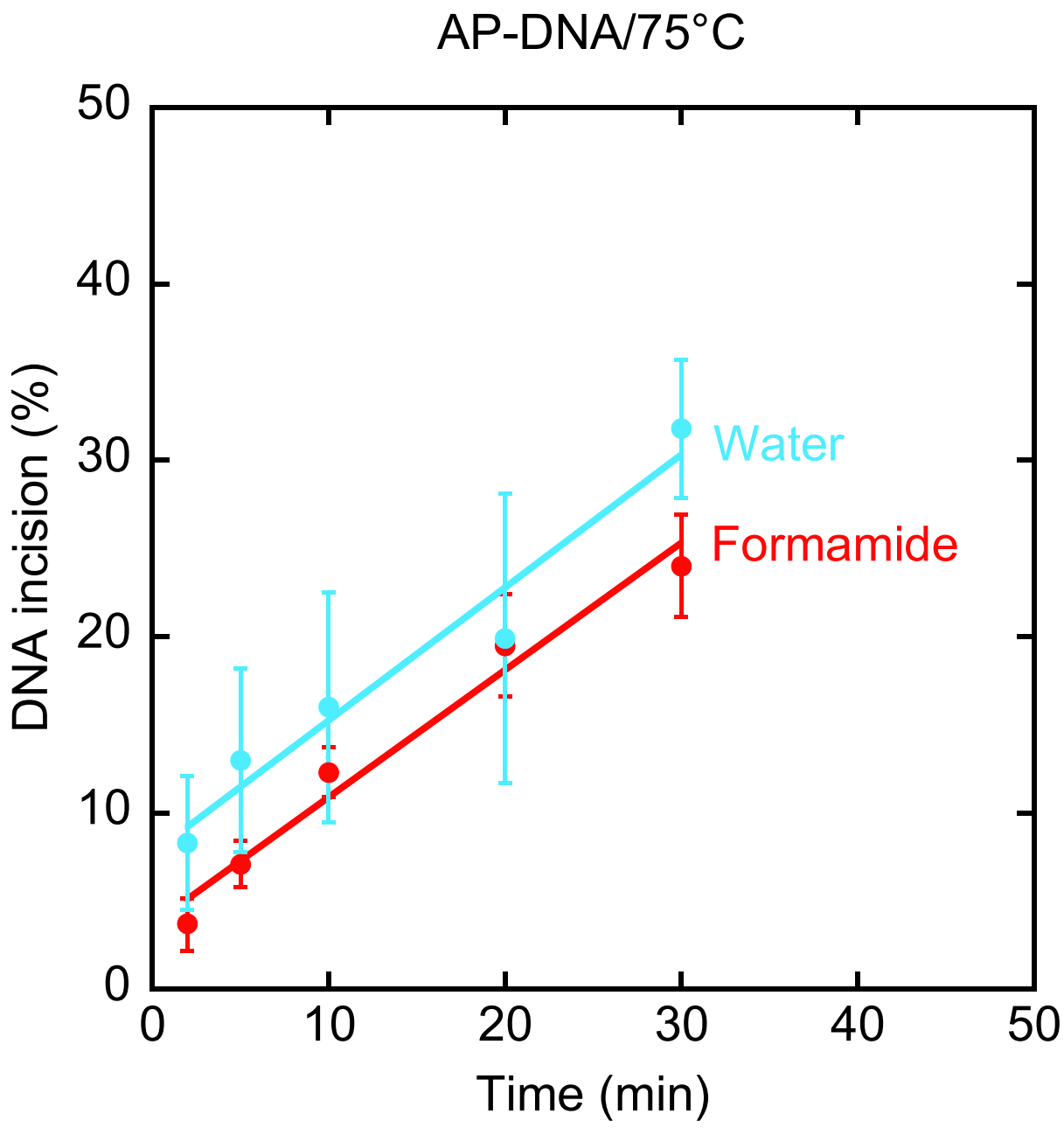
AP-DNA/75°C
DNA incision (%)
Time (min)
Water
Formamide
0
10
20
30
40
50

Fig. 3

A

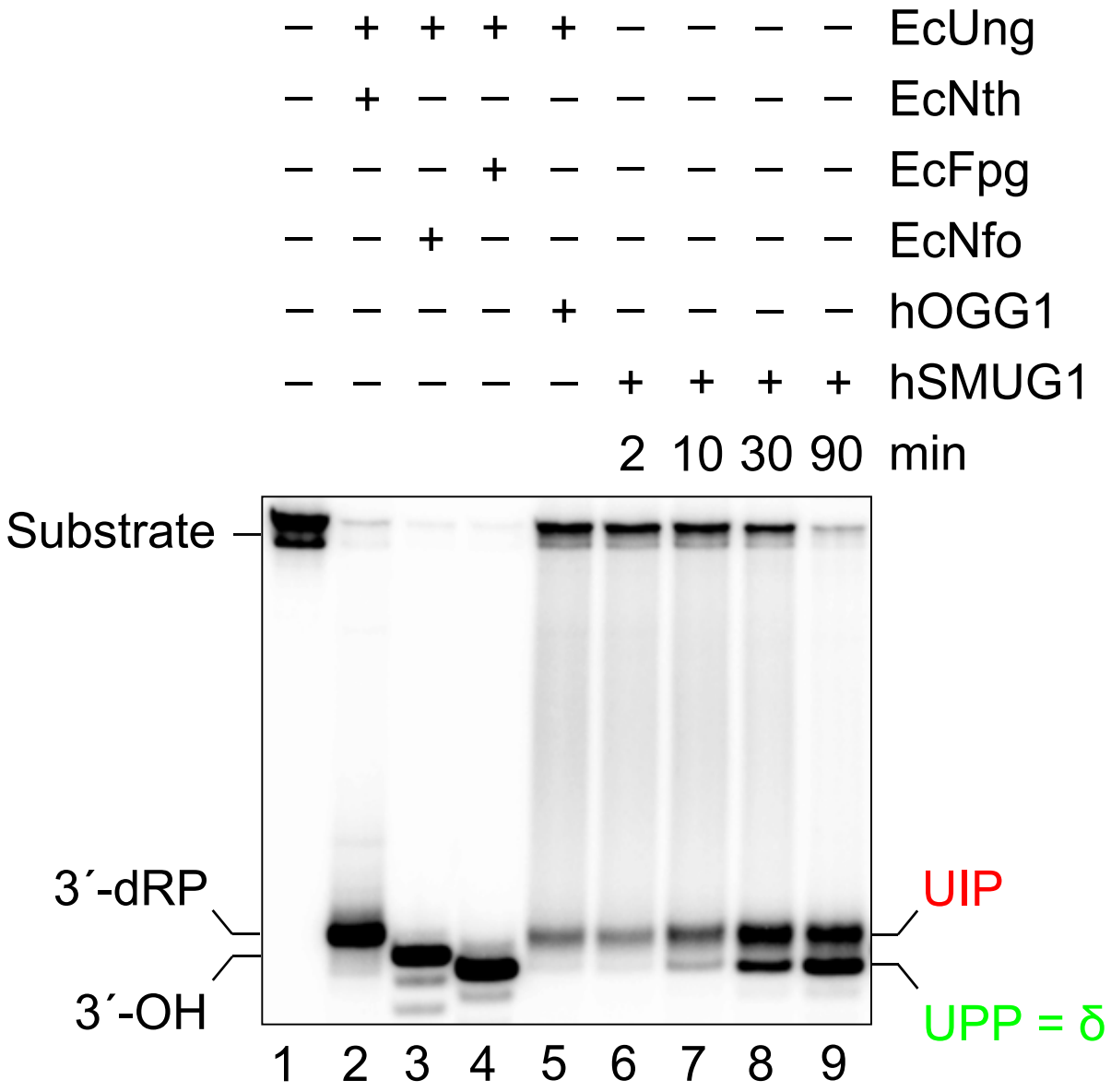
– + + + + – – – – EcUng
– + – – – – – – – EcNth
– – – + – – – – – EcFpg
– – + – – – – – – EcNfo
– – – – + – – – – hOGG1
– – – – – + + + + hSMUG1
2 10 30 90 min
Substrate
3´-dRP
3´-OH
UIP
UPP = δ
1 2 3 4 5 6 7 8 9

Fig. 3

B

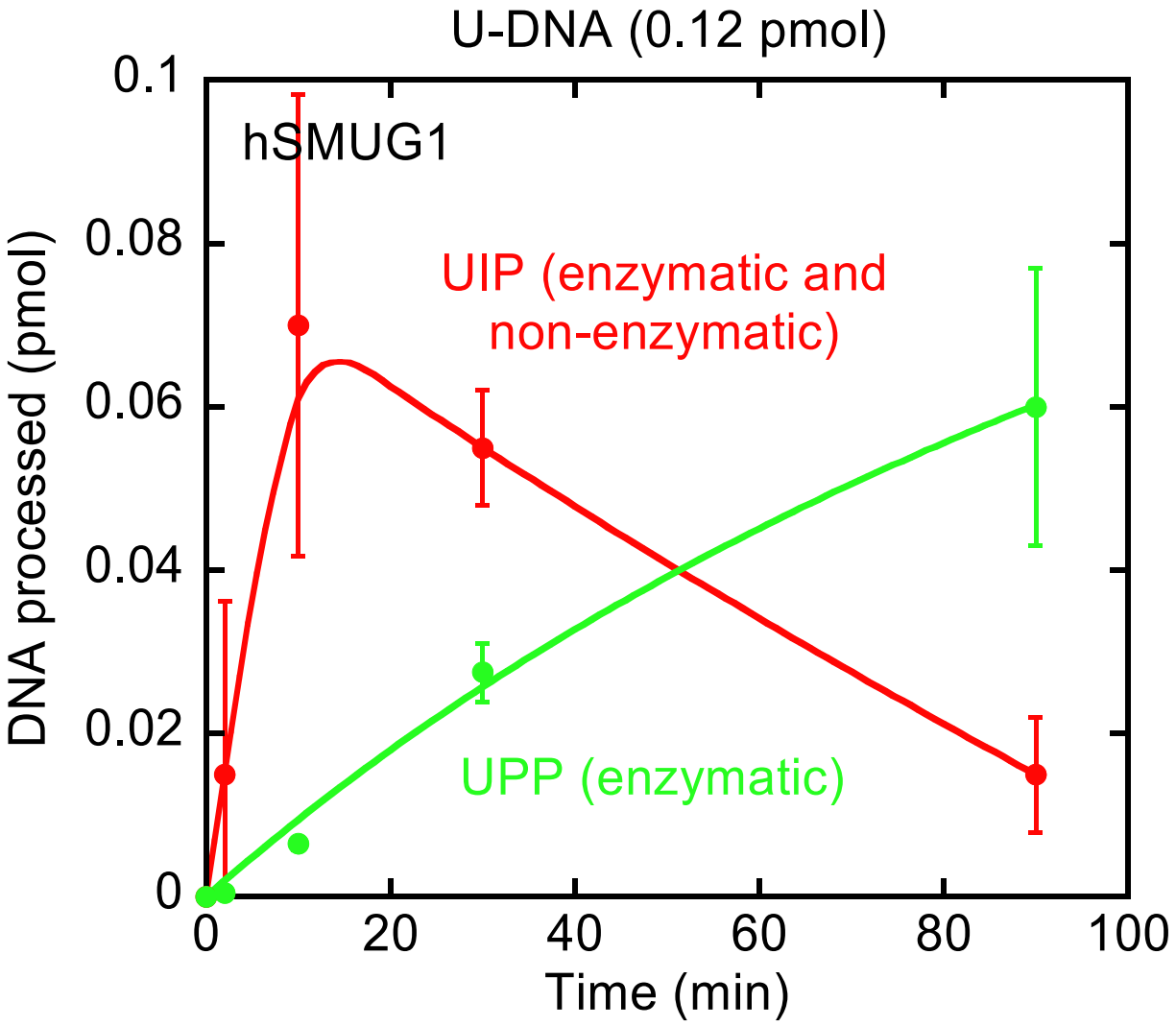
U-DNA (0.12 pmol)
hSMUG1
UIP (enzymatic and non-enzymatic)
UPP (enzymatic)
DNA processed (pmol)
Time (min)
0
0.02
0.04
0.06
0.08
0.1
0
20
40
60
80
100

A

Fig. 4

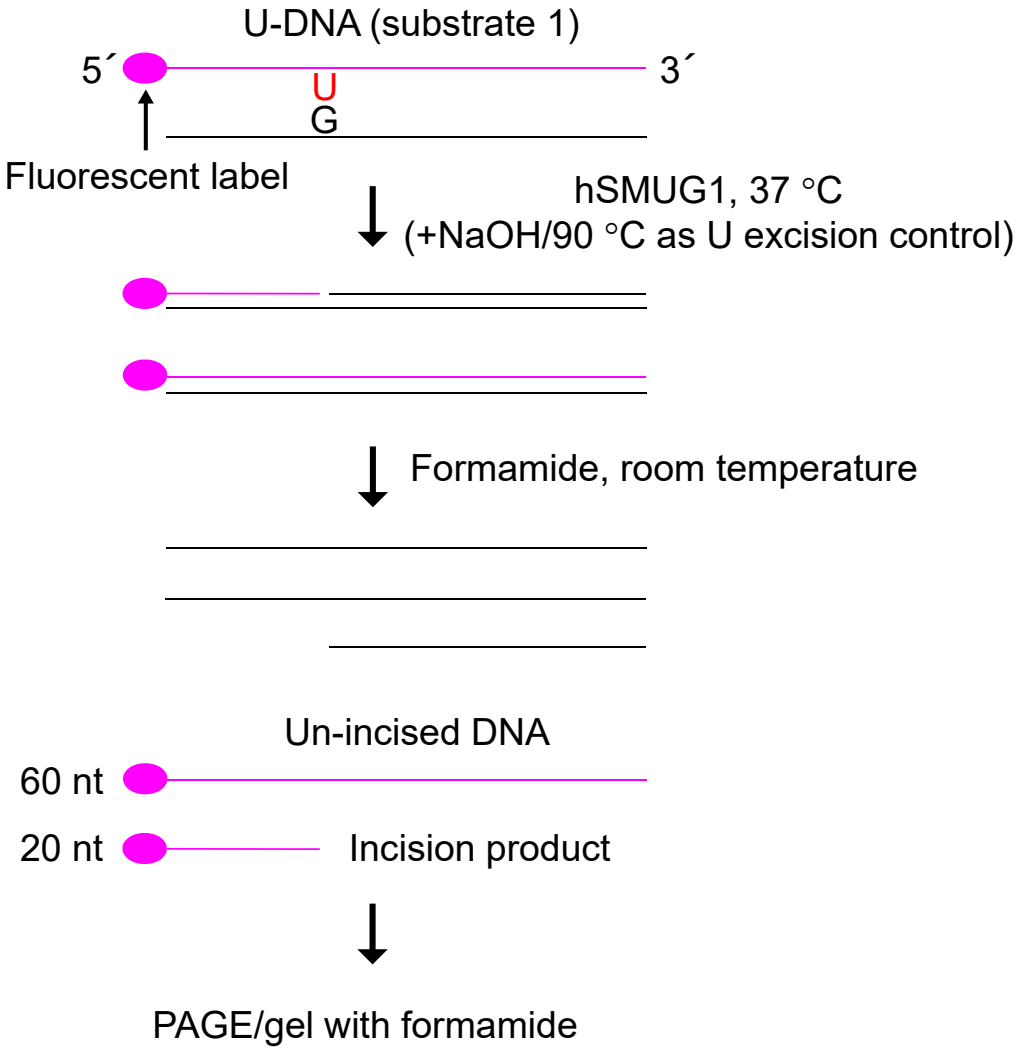
U-DNA (substrate 1)
5´
3´
U
G
Fluorescent label
hSMUG1, 37 °C
(+NaOH/90 °C as U excision control)
Formamide, room temperature
Un-incised DNA
60 nt
20 nt
Incision product
PAGE/gel with formamide

B

Fig. 4

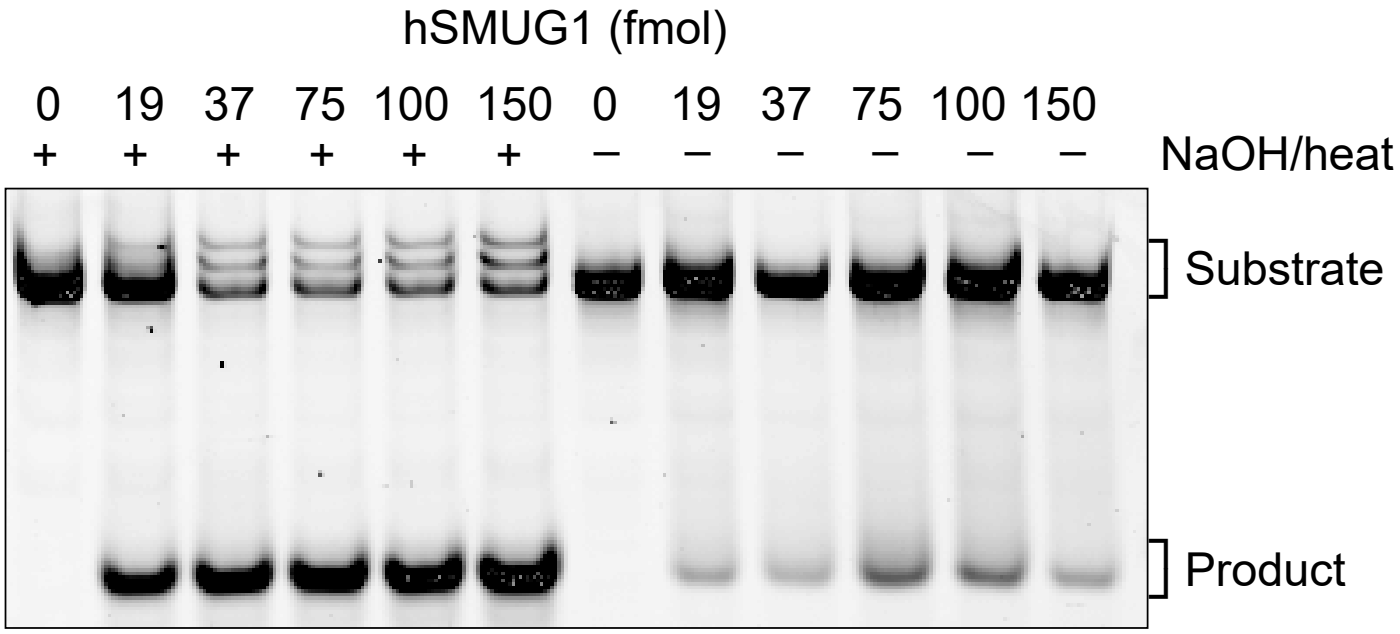
hSMUG1 (fmol)
0 19 37 75 100 150 0 19 37 75 100 150
+ + + + + + – – – – – –
NaOH/heat
Substrate
Product

C

Fig. 4

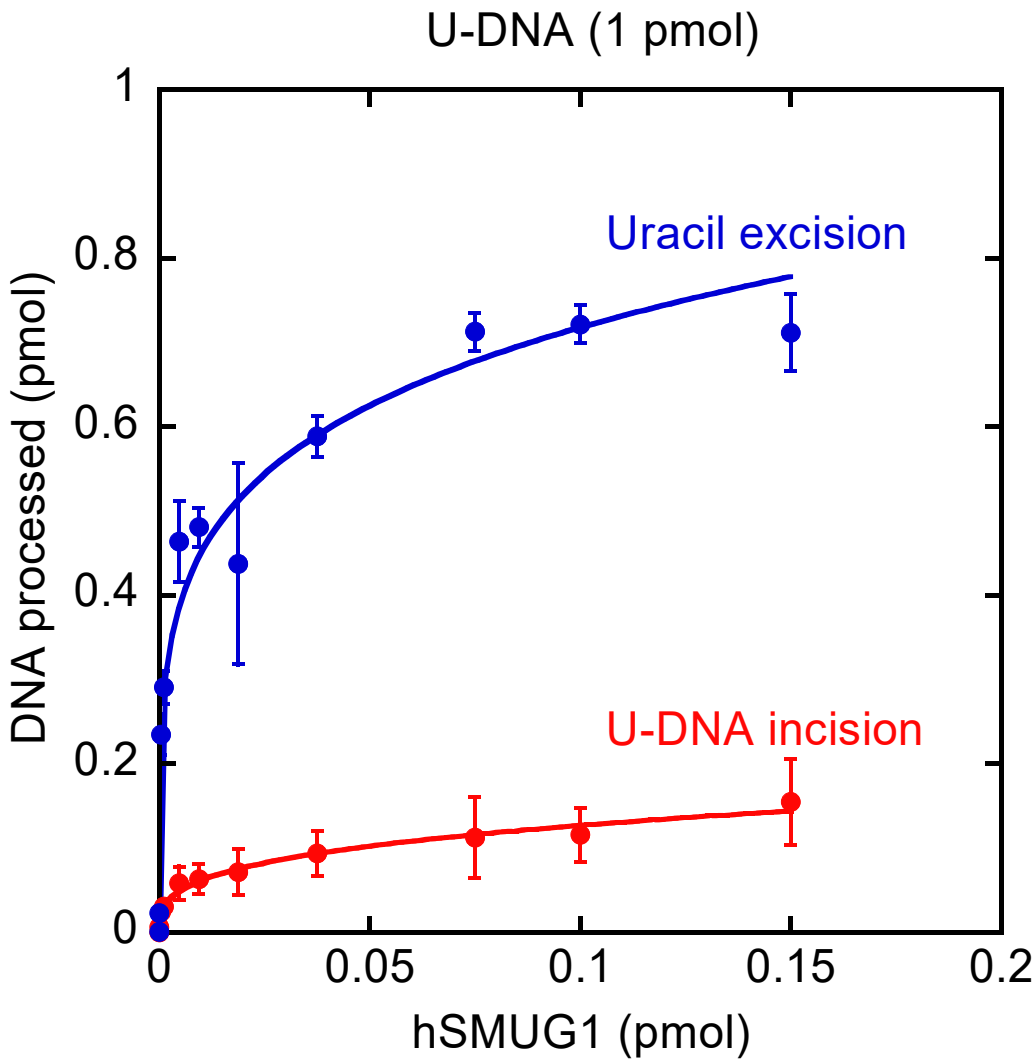
U-DNA (1 pmol)
DNA processed (pmol)
hSMUG1 (pmol)
Uracil excision
U-DNA incision
0
0.2
0.4
0.6
0.8
1
0
0.05
0.1
0.15
0.2

D

Fig. 4

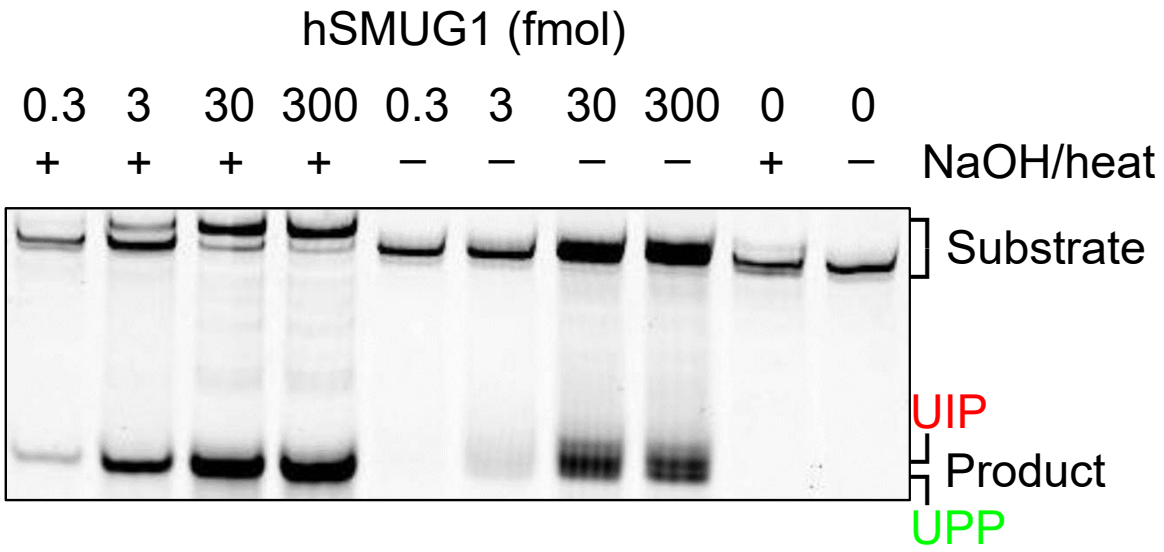
hSMUG1 (fmol)
0.3 3 30 300 0.3 3 30 300 0 0
+ + + + – – – – + –
NaOH/heat
Substrate
UIP
Product
UPP

E

Fig. 4

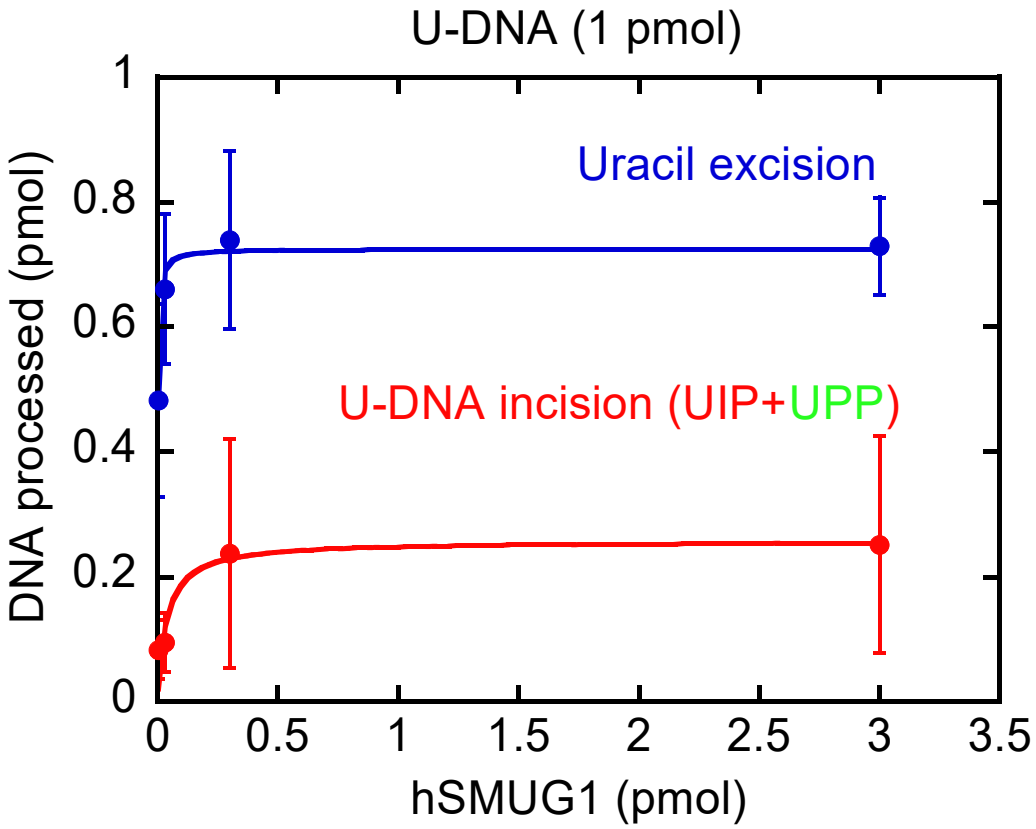
U-DNA (1 pmol)
Uracil excision
U-DNA incision (UIP+UPP)
DNA processed (pmol)
hSMUG1 (pmol)
0
0.2
0.4
0.6
0.8
1
0
0.5
1
1.5
2
2.5
3
3.5

F

Fig. 4

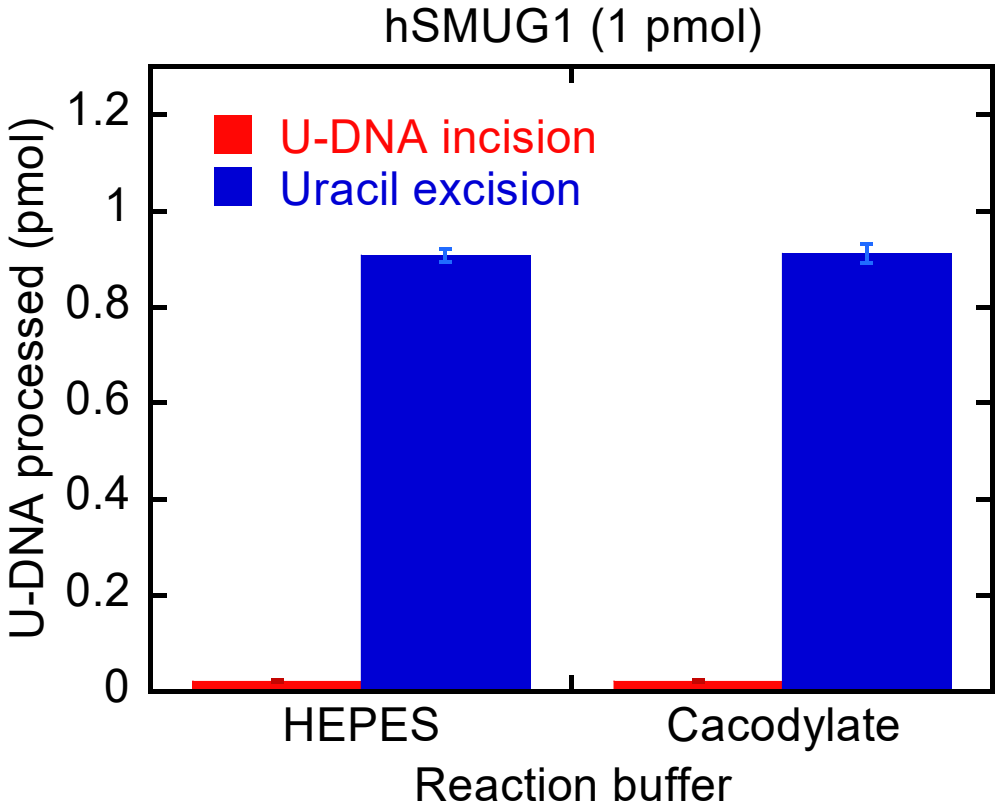
hSMUG1 (1 pmol)
U-DNA incision
Uracil excision
U-DNA processed (pmol)
1.2
1
0.8
0.6
0.4
0.2
0
HEPES
Cacodylate
Reaction buffer

A

Fig. 5

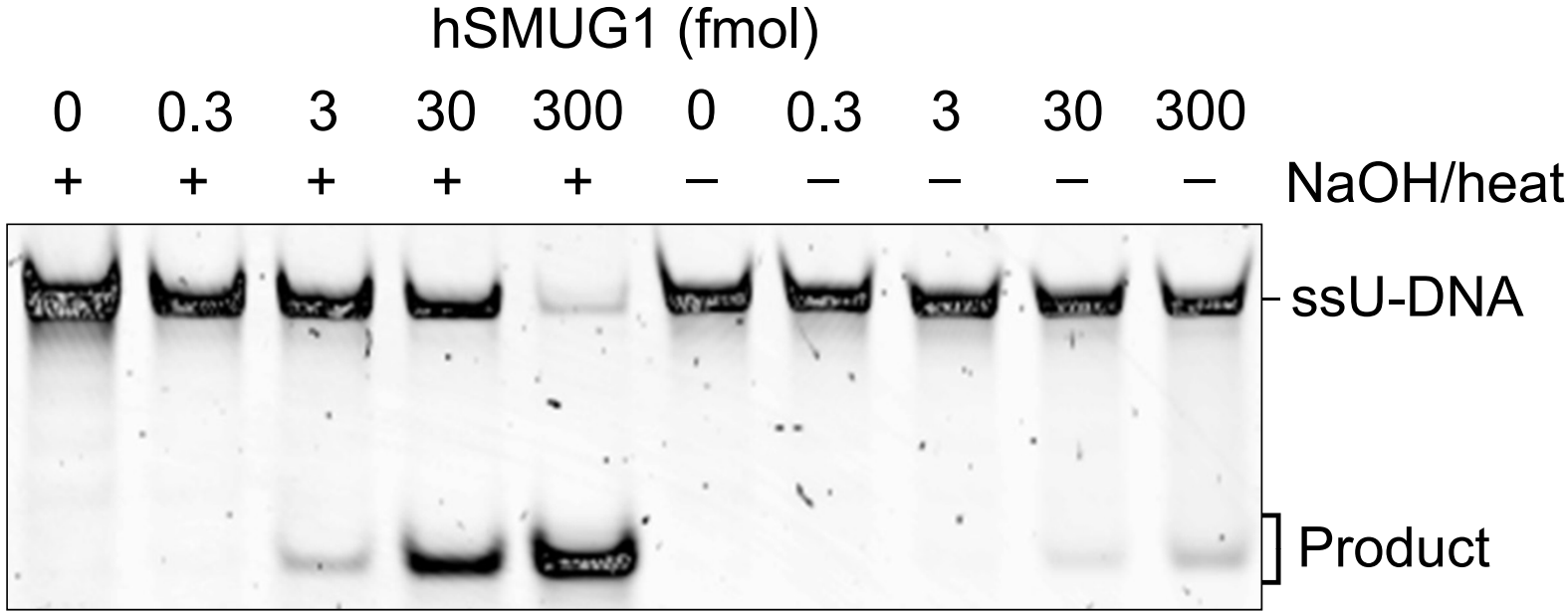

B

Fig. 5

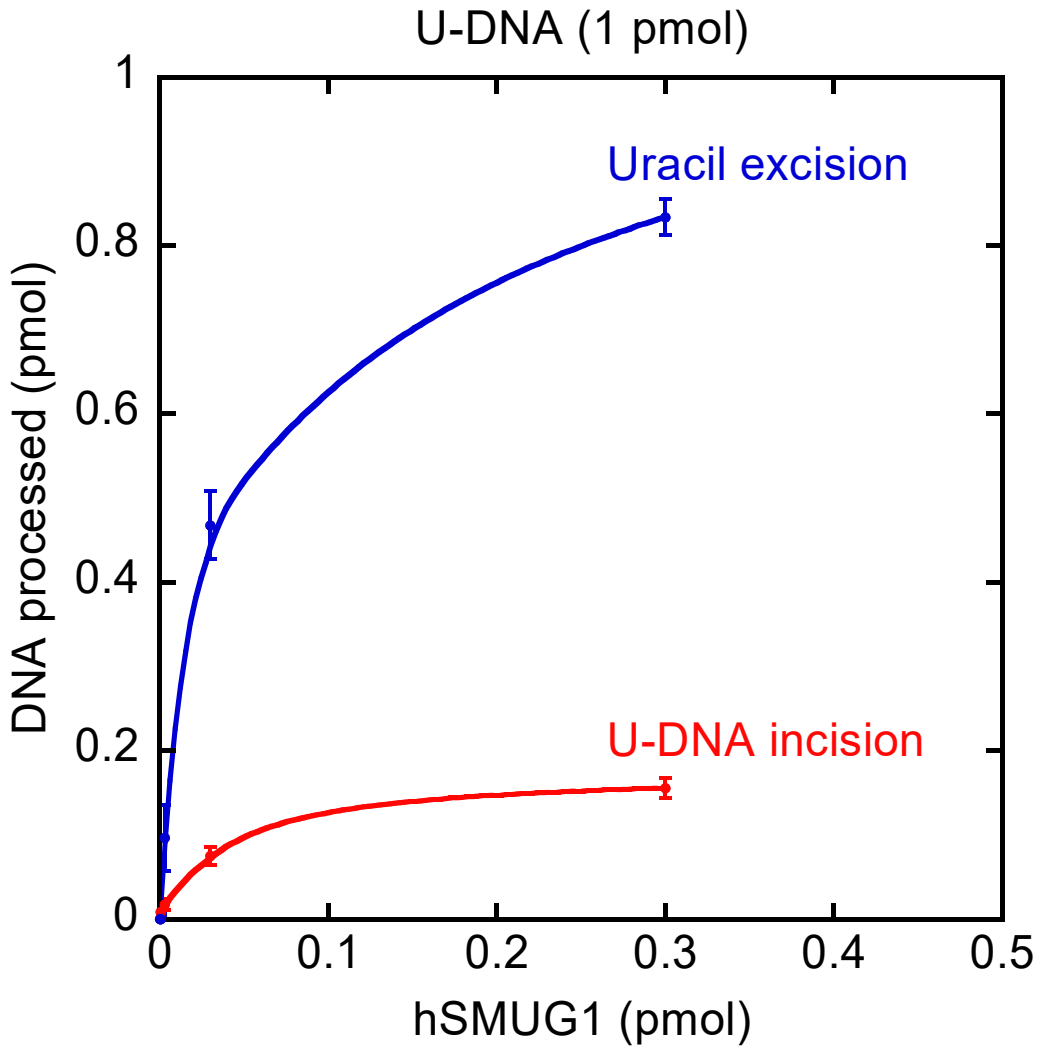
U-DNA (1 pmol)
Uracil excision
U-DNA incision
DNA processed (pmol)
hSMUG1 (pmol)
0
0.2
0.4
0.6
0.8
1
0
0.1
0.2
0.3
0.4
0.5

Fig. 6

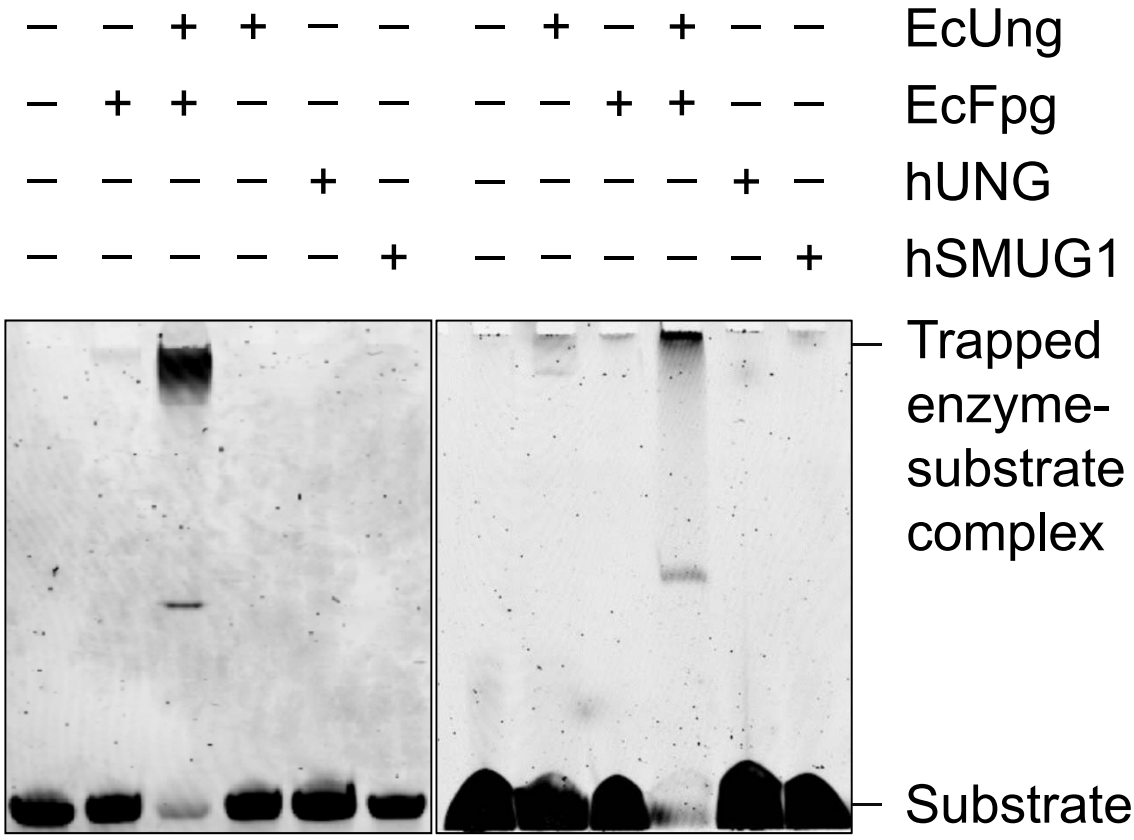
– – + + – – – + – + – – EcUng
– + + – – – – – + + – – EcFpg
– – – – + – – – – – + – hUNG
– – – – – + – – – – – + hSMUG1
Trapped enzyme-substrate complex
Substrate

Fig. 7

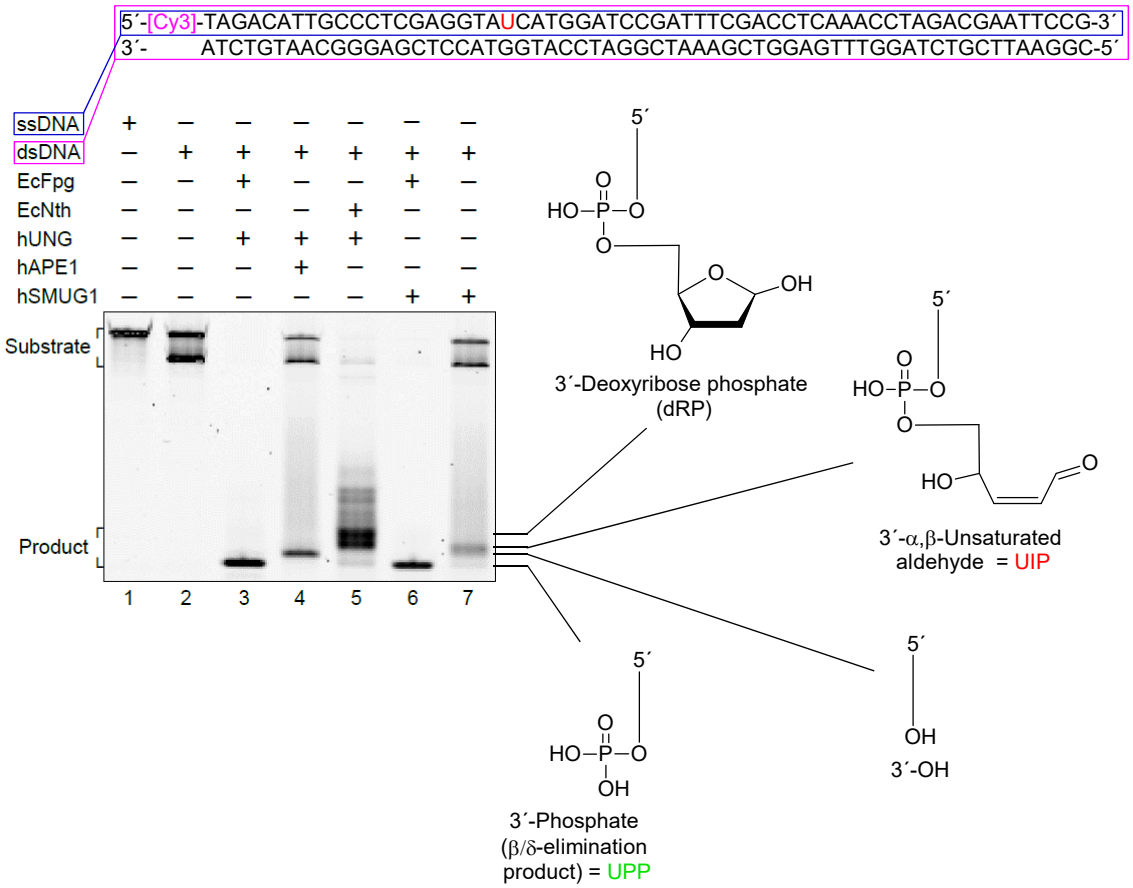
5′-[Cy3]-TAGACATTGCCCTCGAGGTAUCATGGATCCGATTTCGACCTCAAACCTAGACGAATTCCG-3′
3′- ATCTGTAACGGGAGCTCCATGGTACCTAGGCTAAAGCTGGAGTTTGGATCTGCTTAAGGC-5′
ssDNA + – – – – – –
dsDNA – + + + + + +
EcFpg – – + – – + –
EcNth – – – – + – –
hUNG – – + + + – –
hAPE1 – – – + – – –
hSMUG1 – – – – – + +
Substrate
Product
1 2 3 4 5 6 7
3′-Deoxyribose phosphate (dRP)
3′-α,β-Unsaturated aldehyde = UIP
3′-Phosphate (β/δ-elimination product) = UPP
3′-OH

A

Fig. 8

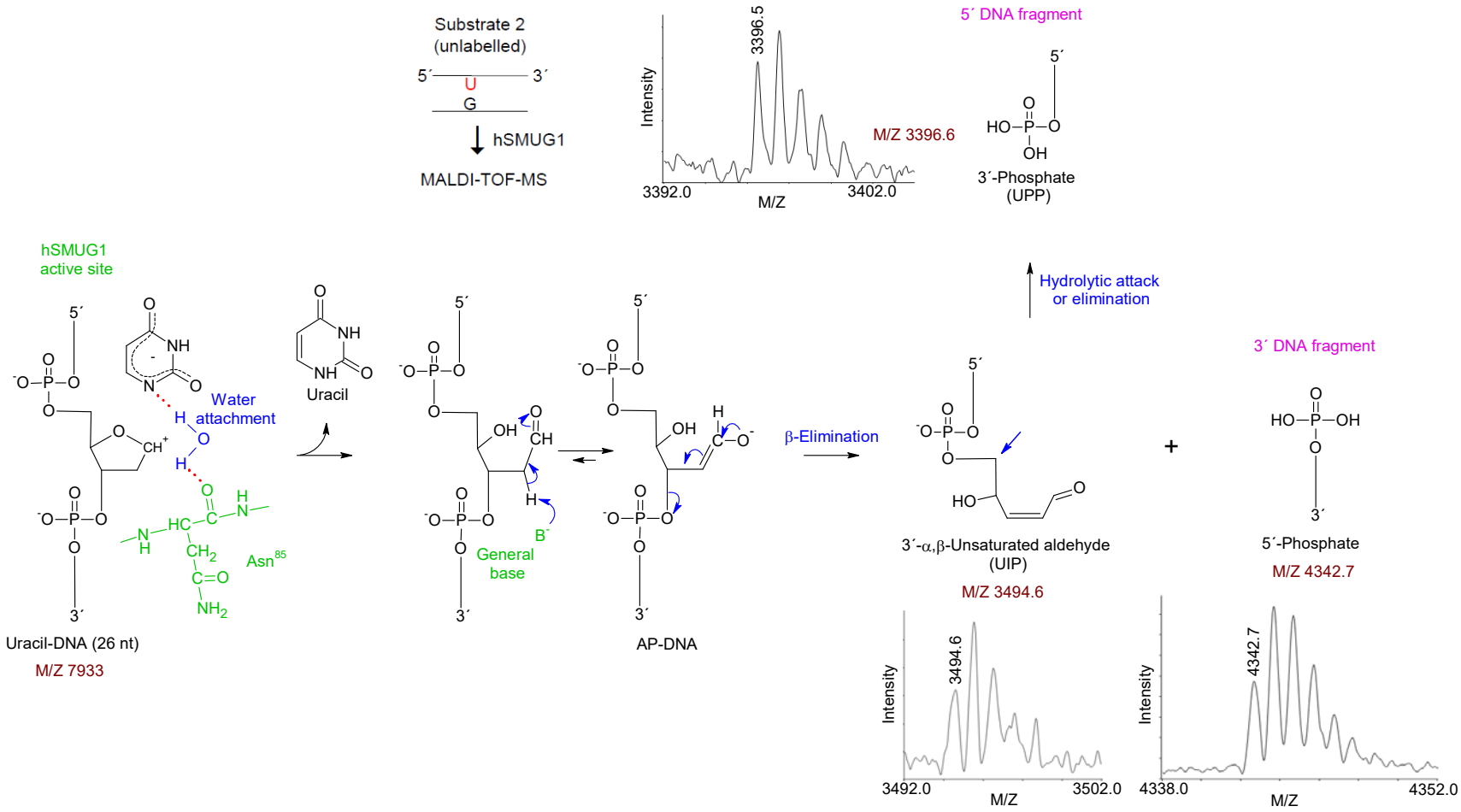
Substrate 2
(unlabelled)
5´
U
G
3´
hSMUG1
MALDI-TOF-MS
Intensity
3396.5
M/Z 3396.6
3392.0
M/Z
3402.0
5´ DNA fragment
HO–P–O
OH
3´-Phosphate
(UPP)
hSMUG1
active site
Water
attachment
Uracil
Uracil-DNA (26 nt)
M/Z 7933
Asn85
General
base
AP-DNA
β-Elimination
Hydrolytic attack
or elimination
3´-α,β-Unsaturated aldehyde
(UIP)
M/Z 3494.6
3´ DNA fragment
5´-Phosphate
M/Z 4342.7
3492.0
3502.0
4338.0
4352.0

B

Fig. 8

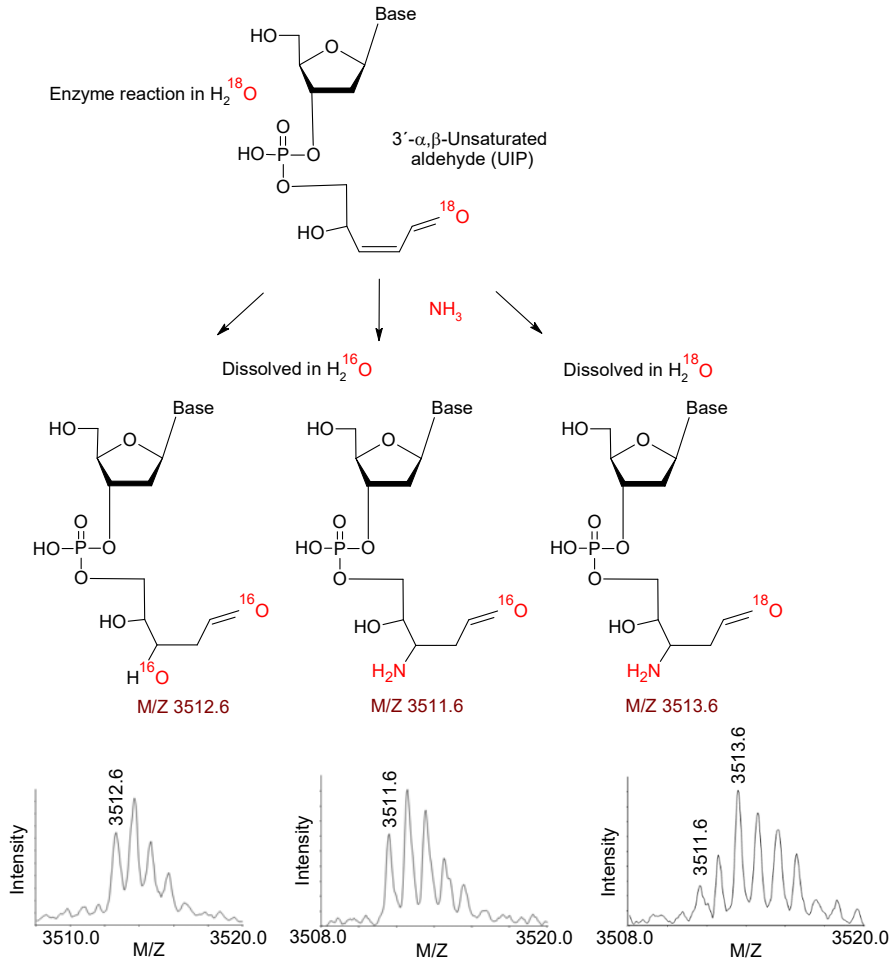
Base
HO
Enzyme reaction in $H_2{}^{18}O$
3´-α,β-Unsaturated aldehyde (UIP)
^{18}O
NH_3
Dissolved in $H_2{}^{16}O$
Dissolved in $H_2{}^{18}O$
^{16}O
$H^{16}O$
H_2N
M/Z 3512.6
M/Z 3511.6
M/Z 3513.6
Intensity
3512.6
3511.6
3513.6
3510.0
3520.0
3508.0
M/Z

A

Fig. 9

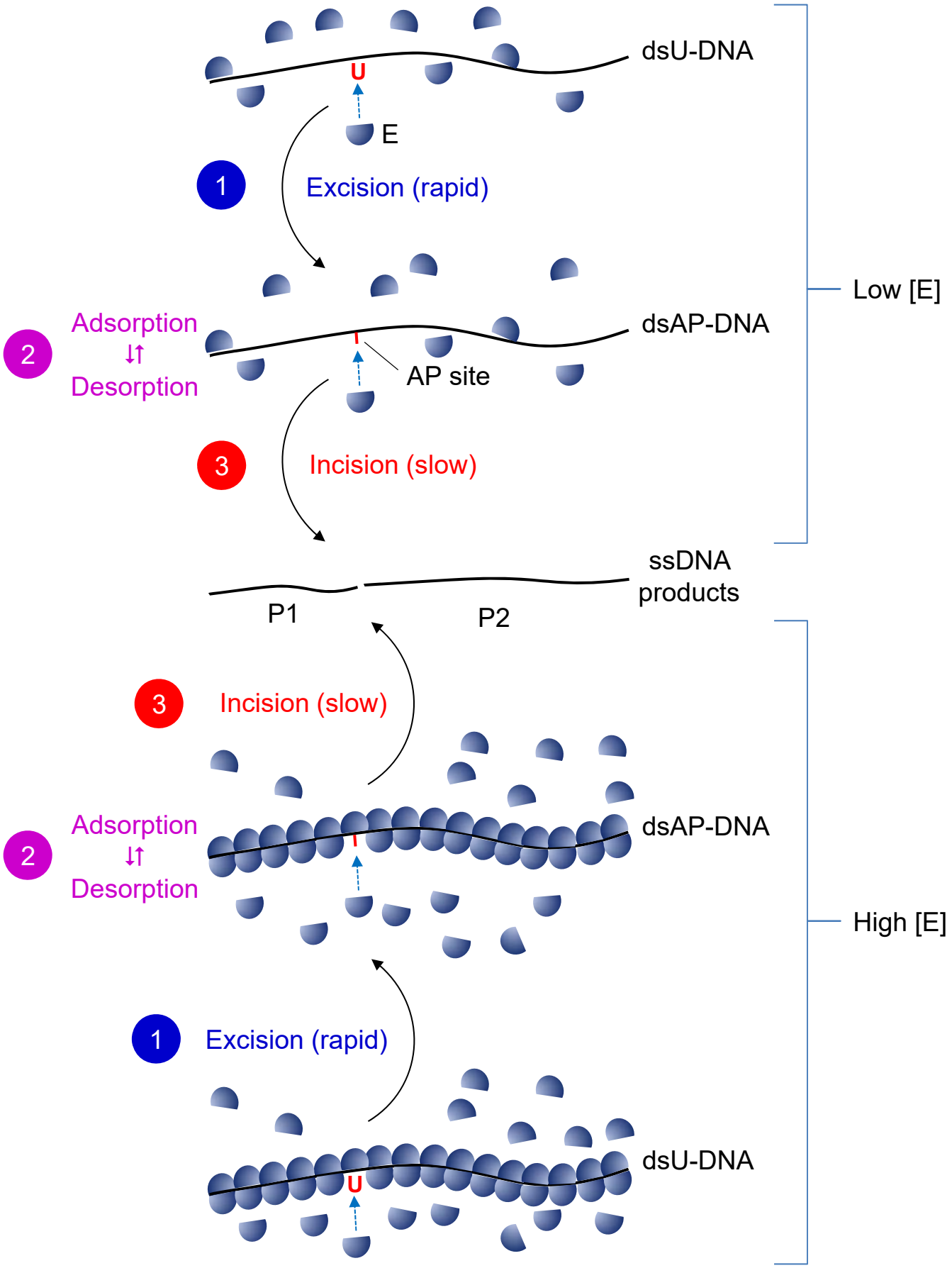
dsU-DNA
U
E
1
Excision (rapid)
Low [E]
Adsorption
Desorption
2
dsAP-DNA
AP site
3
Incision (slow)
ssDNA
products
P1
P2
3
Incision (slow)
Adsorption
Desorption
2
dsAP-DNA
High [E]
1
Excision (rapid)
dsU-DNA
U

Fig. 9

B

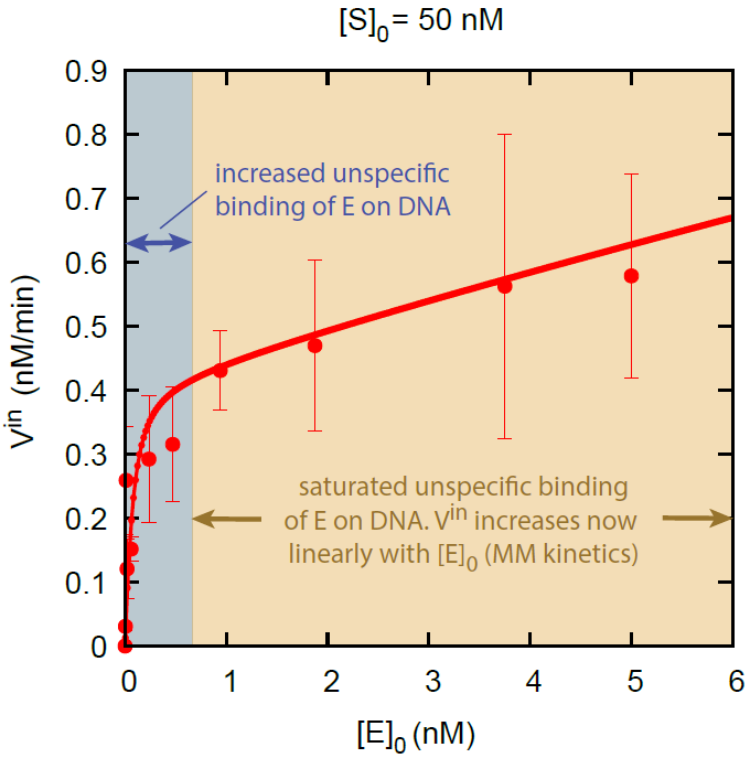
[S]0 = 50 nM
increased unspecific binding of E on DNA
saturated unspecific binding of E on DNA. Vin increases now linearly with [E]0 (MM kinetics)
Vin (nM/min)
[E]0 (nM)
0
0.1
0.2
0.3
0.4
0.5
0.6
0.7
0.8
0.9
0
1
2
3
4
5
6

C

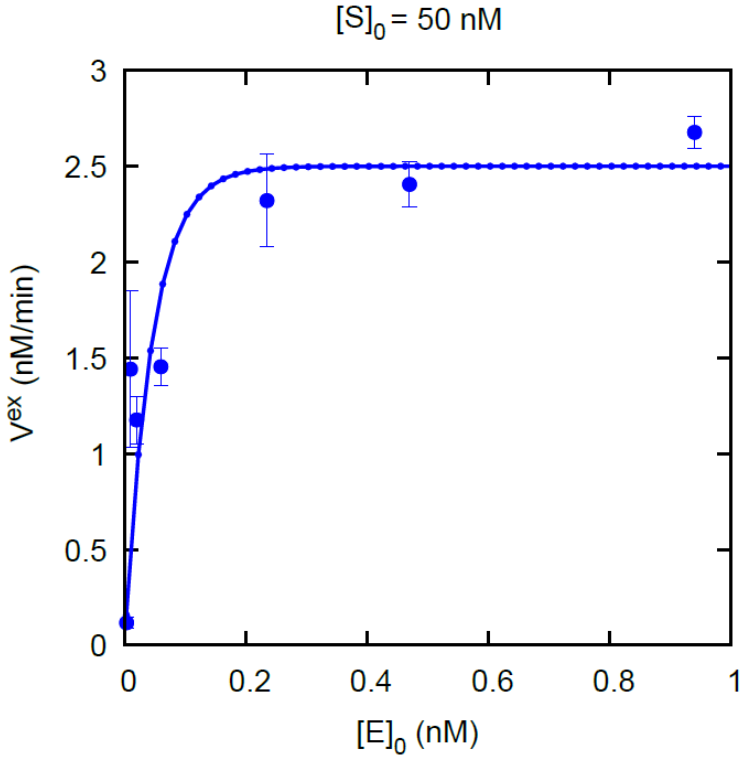
[S]0 = 50 nM
Vex (nM/min)
[E]0 (nM)
0
0.5
1
1.5
2
2.5
3
0
0.2
0.4
0.6
0.8
1

Fig. 9

D

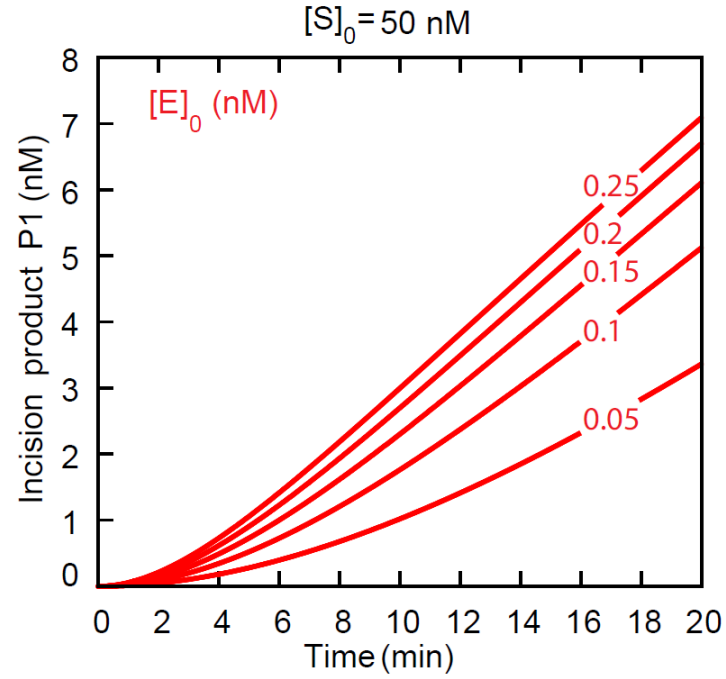
[S]0 = 50 nM
[E]0 (nM)
0.25
0.2
0.15
0.1
0.05
Incision product P1 (nM)
Time (min)

E

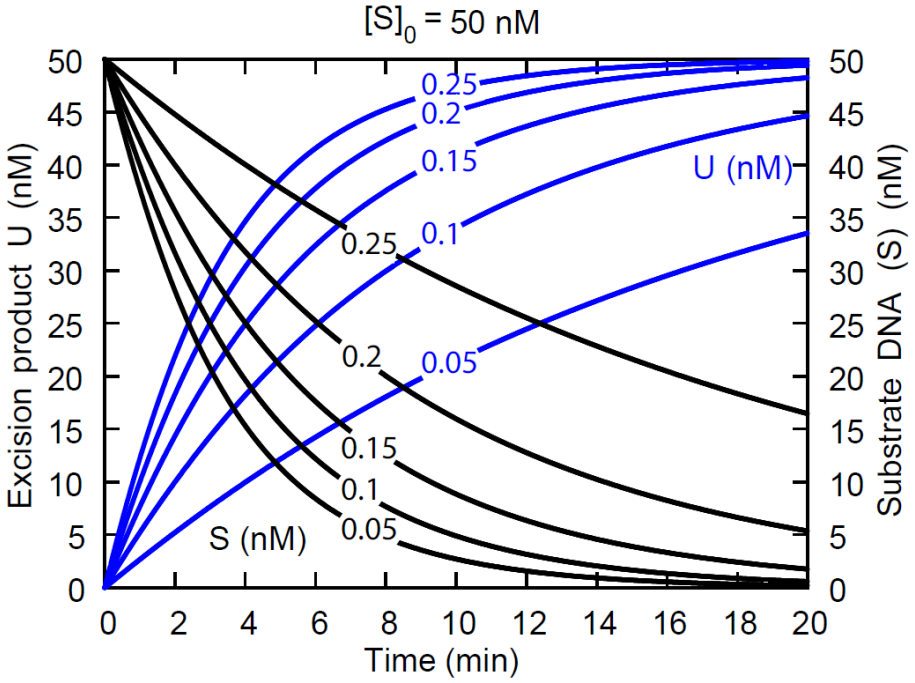
[S]0 = 50 nM
U (nM)
S (nM)
0.25
0.2
0.15
0.1
0.05
Excision product U (nM)
Substrate DNA (S) (nM)
Time (min)

Fig. 10

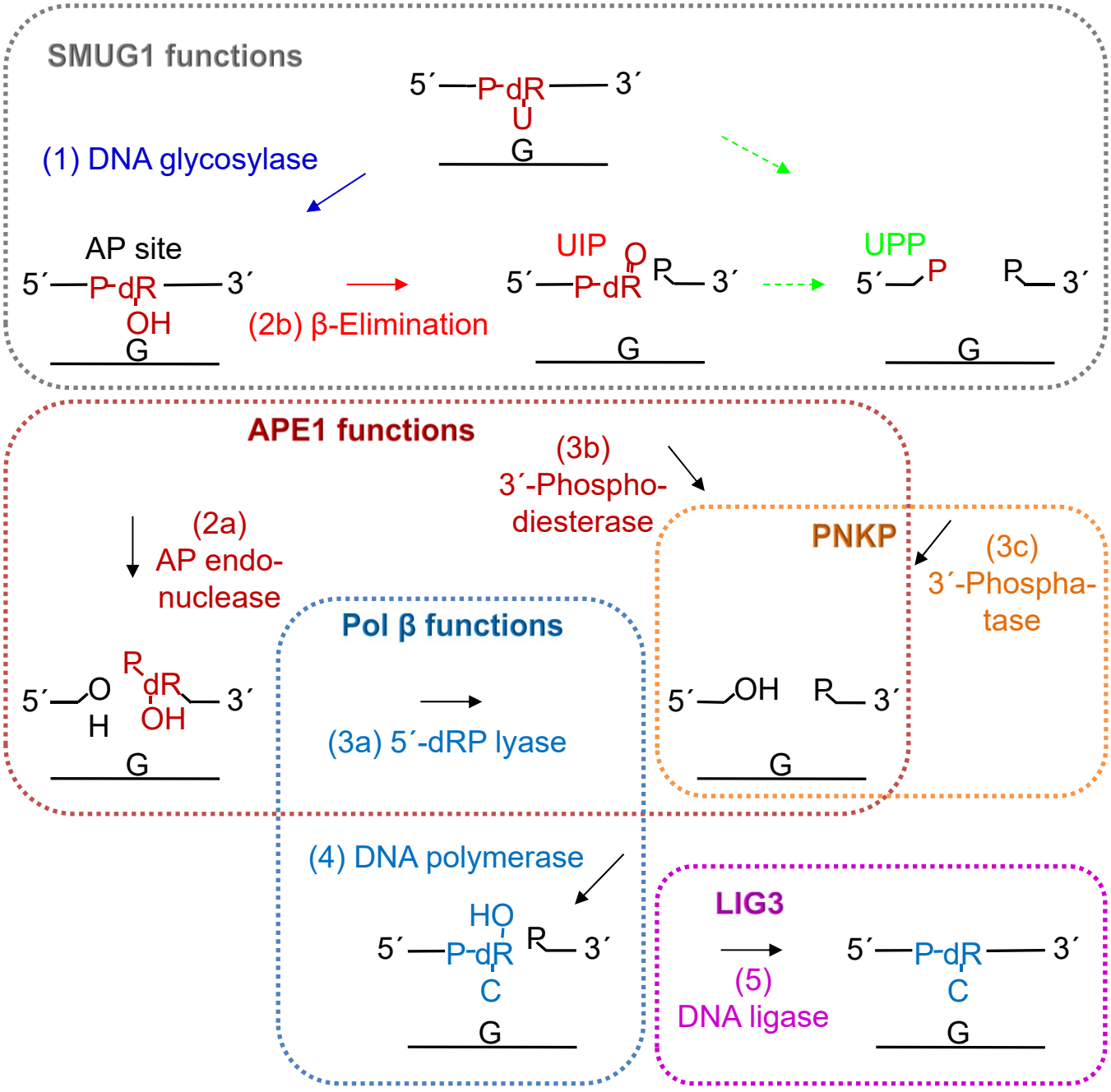
SMUG1 functions
5′—P-dR—3′
U
G
(1) DNA glycosylase
AP site
5′—P-dR—3′
OH
G
(2b) β-Elimination
UIP
O
5′—P-dR
P—3′
G
UPP
5′—P
P—3′
G
APE1 functions
(3b)
3′-Phospho-
diesterase
PNKP
(3c)
3′-Phospha-
tase
(2a)
AP endo-
nuclease
Pol β functions
R
5′—O
H
dR
OH
3′
G
(3a) 5′-dRP lyase
5′—OH
R—3′
G
(4) DNA polymerase
HO
5′—P-dR
R—3′
C
G
LIG3
(5)
DNA ligase
5′—P-dR—3′
C
G

Supplementary Data

Alexeeva et al.

Comment on β-elimination products produced by EcNth and hOGG1

Our preparation of the samples for PAGE at room temperature, instead of at the complete denaturing conditions at 95 °C, caused no difference in electrophoretic mobility between the 5′ incision fragments formed by EcFpg and EcNfo/hAPE1 (Figures 3A and 7). In contrast, for EcNth the conventional 95 °C-treatment resulted in one major band defining the 3′-dRP (Figure 3A) whereas the room temperature treatment resulted in two bands corresponding to both the 3′-dRP and the 3′-α,β-unsaturated aldehyde ends (Figure 7). For hOGG1 we observed the same bands although the 3′-α,β-unsaturated aldehyde tended to be the major product (data not shown). This accords with previous results indicating that hOGG1 (1,2) as well as EcNth (3) form two to several β-elimination products. EcNth and hOGG1 incise AP sites by a β-elimination reaction resulting in similar enzyme-substrate intermediates (3-11). However, the atomic site of subsequent water addition and/or whether one or two water molecules are added may determine whether the result is a 3′-dRP or a 3′-α,β-unsaturated aldehyde (12). Spontaneous interchange (dehydration/hydration) between the two forms may also complicate interpretation of results.

A three-phase kinetic model

Theoretical and experimental arguments for a three-phase model

We developed a model describing the hSMUG1 (E) kinetics of uracil excision and U-DNA incision in three phases/stages (Figure 9A), which corresponds well with the experimental data (Figures 9B, 9C and Supplementary Data, Figure S5).

Phase 1: Rapid uracil excision. In the first stage, E binds DNA_U and rapidly releases U to form DNA_{AP}. As a simplification, we avoid considering a reversible binding between DNA and E, which leads to the overall excision reaction

$$E + DNA_U \xrightarrow{k_1} DNA_{AP} \cdot U \cdot E \xrightarrow{k_p^{ex}} DNA_{AP} + U + E \qquad (1)$$

To determine the rate constants k_1 and k_p^{ex} we used an initial U-DNA concentration [DNA_U] of 50 mM and adjusted the constants to the best "eye-balled" fit (see Figure 9C). The values of k_1 (1.5 nM^{-1} min^{-1}) and k_p^{ex} obtained were kept in later calculations with more processes added to the model and at higher initial [DNA_U]. The velocity V^{ex} is calculated as [DNA_{AP}] (which equals [U] released) divided by the 20 min assay time, *i.e.*

$$V^{ex} = [DNA_{AP}]/20 \text{ (nM/min)} \qquad (2)$$

Note that the 2.5 nM/min-level in Figure 9C does not results from enzyme saturation, but reflects that all of the 50 nM DNA_U is processed within the 20 min assay time resulting in the maximal V^{ex}. The excision reaction is relatively rapid, indicating that an [E] of 0.2 nM processes all initial DNA within 20 min.

Phase 2: Slow adsorption/desorption of enzyme to DNA. Reaction (1) shows that DNA_{AP} forms together with (free) U. The model assumes that E binds and dissociates randomly and non-specifically at different places on DNA_{AP}. At low [E], few E molecules are adsorbed on the DNA_{AP} surface, while at higher [E], the DNA_{AP} is more densely populated by E which continuously adsorbs and desorbs (Figure 9A). Whenever E binds at the AP or cleavage site DNA_{AP} cleaves into P1 and P2. The kinetics of the enzyme adsorption/desorption process can be described as

$$E + DNA_{AP,\,j\neq i} \underset{k_{-1}}{\overset{k_1}{\rightleftharpoons}} E \cdot DNA_{AP,\,j\neq i} \qquad (3)$$

Where *j* is any site on DNA except the incision site *i*. If it we assume that a single DNA_{AP} molecule has *N* unspecific binding sites for E, with n_{empty} describing the number of sites without E, while n_{occ} describes the sites on DNA_{AP} occupied by E, it gives

$$n_{occ} + n_{empty} = N \qquad (4)$$

The rate of adsorption is dependent on the number of vacant sites, n_{empty}, and the concentration of E in the solution, *i.e.*

$$V^{adsorp} = k_1 \cdot n_{empty} \cdot [E] \qquad (5)$$

The rate of desorption, in contrast, is determined by the number of E-occupied sites only, *i.e.*

$$V^{desorp} = k_{-1} \cdot n_{occ} \qquad (6)$$

At steady state/dynamical equilibrium

$$V^{adsorp} = V^{desorp} \qquad (7)$$

Using Θ instead for n_{occ} we write at steady state

$$k_{-1} \cdot \Theta_{ss} = k_1 \cdot (N - \Theta_{ss})\,[E] \qquad (8)$$

which solved for Θ_{ss} gives

$$\Theta_{ss} = k_1 \cdot N \cdot [E]/(k_{-1} + k_1 \cdot [E]) = N \cdot [E]/(K_D + [E]) \text{ where } K_D = k_1/k_{-1} \qquad (9)$$

and shows that the number of E-occupied sites follows a saturation curve in [E], also called an *adsorption isotherm* (13).

Since E only bound to the AP or incision site *i* leads to cleavage of DNA_{AP},

$$E + DNA_{AP,\,i} \rightleftharpoons E \cdot DNA_{AP,\,i} \xrightarrow{k_1^{in}} E + P1 + P2 \qquad (10)$$

it is needed to calculate the probability that E binds at site *i*. The simplest assumption is that the binding probability $\mathcal{P}$ is equal for the *N* sites. In that case, the probability $\mathcal{P}$ that E binds at the site *i* for a single DNA_{AP} molecule (or one mole DNA_{AP}) is

$$\mathcal{P} = \Theta_{ss}/N = [E]/(K_D + [E]) \qquad (11)$$

Thus, the reaction rate for cleaving DNA_{AP} to form P1, while E is still adsorbing at empty binding sites on DNA_{AP}, is

$$V^{in} = V_1^{in} = k_1^{in} \cdot [DNA_{AP}]\,([E]/(K_D + [E])) \qquad (12)$$

Equation (12) describes the rate of formation of the measured product P1 during the adsorption/desorption phase 2 (Figure 9A).

Phase 3: Slow incision of AP site. With increasing initial [E], E eventually occupies all binding sites on DNA_{AP}, *i.e.*, DNA_{AP} is saturated with adsorbed E and no more E will bind. However, at the AP site, E cleaves DNA and the rate of cleavage is (approximately) proportional to $[DNA_{AP} \cdot E]$ (the latter denotes the concentration of DNA_{AP} saturated with adsorbed E molecules; Figure 9A), giving

$$E + DNA_{AP} \xrightarrow{k_2} DNA_{AP} \cdot E \xrightarrow{k_2^{in}} P1 + P2 + E \qquad (13)$$

where k_2 was determined as 0.002 $nM^{-1}\ min^{-1}$. To simplify, we have neglected the nonreactive dissociation of $DNA_{AP} \cdot E$ back to E and DNA_{AP}, as formulated in Equation (10). Considering

the first step as irreversible, the cleavage rate of DNA_{AP} to produce P1 under saturating conditions of E is

$$V_2^{in} = k_2^{in} \cdot [DNA_{AP} \cdot E] \qquad (14)$$

Overview of the kinetic model

The model describes the hSMUG1 (E) excision/incision kinetics during three phases/stages (Figure 9A). First, a rapid initial uracil excision phase 1 occurs and converts the U site into an AP site resulting in $DNA_U \rightarrow DNA_{AP}$. A less reactive phase 2 follows when E binds non-specifically at different sites including the AP site. When bound to the AP site E induces cleavage of DNA_{AP}, which leads to the products P1 and P2 and the release of E. In the final phase 3, high [E] saturates DNA_{AP} because E binds at the nonreactive sites forming a dynamic equilibrium (steady state). Further changes in [E] are only affecting the rate of cleavage when E binds to the AP site.

The following set of reactions/equations describes the model:

$$E + DNA_U \xrightarrow{k_1} DNA_{AP} \cdot U \cdot E \xrightarrow{k_p^{ex}} DNA_{AP} + U + E \qquad (1)$$

$$DNA_{AP} \xrightarrow[k_1^{in},\, K_D]{E} P1 + P2 \qquad (15)$$

with $$V_1^{in} = k_1^{in} \cdot [DNA_{AP}] \cdot ([E]/(K_D + [E])) \qquad (16)$$

and $$E + DNA_{AP} \xrightarrow{k_2} DNA_{AP} \cdot E \xrightarrow{k_2^{in}} P1 + P2 + E \qquad (13)$$

The total formation rate of P1 (the measured product UIP) is

$$\left(\frac{d[P1]}{dt}\right)_{total} = \overbrace{k_1^{in} \cdot [DNA_{AP}] \cdot ([E]/(K_D + [E]))}^{V_1^{in}\text{(competition with unspecific binding sites)}} + \overbrace{k_2^{in} \cdot [DNA_{AP} \cdot E]}^{V_2^{in}\text{(E saturated at unspecific binding sites)}} \qquad (17)$$

The excision rate of uracil is

$$\frac{d[U]}{dt} = k_p^{ex} \cdot [DNA_{AP} \cdot U \cdot E] \qquad (18)$$

The other rate equations are:

$$\frac{d[\mathrm{E}]}{dt} = -\mathrm{k}_1\,[\mathrm{E}]\cdot\left[\mathrm{DNA_U}\right] + \mathrm{k_p^{ex}}[\mathrm{DNA_{AP}}\cdot\mathrm{U}\cdot\mathrm{E}] - \mathrm{k}_2\,[\mathrm{E}]\cdot\left[\mathrm{DNA_{AP}}\right] + \mathrm{k_2^{in}}[\mathrm{DNA_{AP}}\cdot\mathrm{E}] \qquad (19)$$

$$\frac{d\left[\mathrm{DNA_U}\right]}{dt} = -\mathrm{k}_1\,[\mathrm{E}]\cdot\left[\mathrm{DNA_U}\right] \qquad (20)$$

$$\frac{d\left[\mathrm{DNA_{AP}\cdot U\cdot E}\right]}{dt} = \mathrm{k}_1\,[\mathrm{E}]\cdot\left[\mathrm{DNA_U}\right] - \mathrm{k_p^{ex}}[\mathrm{DNA_{AP}}\cdot\mathrm{U}\cdot\mathrm{E}] \qquad (21)$$

$$\frac{d\left[\mathrm{DNA_{AP}}\right]}{dt} = \mathrm{k_p^{ex}}[\mathrm{DNA_{AP}}\cdot\mathrm{U}\cdot\mathrm{E}] - \mathrm{k}_2\,[\mathrm{E}]\cdot\left[\mathrm{DNA_{AP}}\right] - \mathrm{k_1^{in}}[\mathrm{DNA_{AP}}]([\mathrm{E}]/(\mathrm{K_D} + [\mathrm{E}])) \qquad (22)$$

The above (rate) equations were solved numerically by using the Fortran subroutine LSODE as described in Materials and Methods.

Discussion

Figures 9B, 9C and Supplementary Data, Figure S5 show a relative good agreement between the calculated and measured values, despite the simplicity of the model. The model predicts that with increasing DNA concentration the number of unspecific binding sites increases proportionally to *N times* the concentration of DNA, while the number of cleavable sites increases only proportionally with the concentration of DNA. If we assume that all binding sites have an equal probability to bind E, then the probability to bind at the cleavable site is the inverse of the number of binding sites. Thus, the rate of $\mathrm{DNA_{AP}}$ cleavage with constant E concentration should be inversely proportional to $N \cdot [\mathrm{DNA}]_0$, *i.e.*

$$k_1^{\mathrm{in}} = \frac{\kappa}{N\cdot[\mathrm{DNA}]_0} \qquad (23)$$

where κ is a constant. Thus, k_1^{in} can be estimated for different initial DNA concentrations once a k_1^{in} value is assigned to an initial DNA concentration. For example, we now assume that $k_1^{\mathrm{in}}([\mathrm{DNA}]_{0.1})$ denotes k_1^{in} at an initial DNA concentration of 0.1 nM, while $k_1^{\mathrm{in}}([\mathrm{DNA}]_{0.2})$ denotes k_1^{in} at an initial DNA concentration of 0.2 nM. If the value of

$k_1^{\text{in}}([\text{DNA}]_{0.1})$ is known, our assumption that E binds non-specifically with equal probability to the *N* binding sites predicts that $k_1^{\text{in}}([\text{DNA}]_{0.2})$ can be calculated according to

$$k_1^{\text{in}}\left([\text{DNA}]_{0.2}\right) = k_1^{\text{in}}\left([\text{DNA}]_{0.1}\right) \cdot \left(\frac{[\text{DNA}]_{0.1}}{[\text{DNA}]_{0.2}}\right) \qquad (24)$$

If we take $[\text{DNA}]_{0.1}$ = 50 nM with a corresponding $k_1^{\text{in}}([\text{DNA}]_{0.1})$ = 0.009 min^{-1}, then the k_1^{in} value for 375 nM is calculated as

$$k_1^{\text{in}}(375\text{ nM}) = k_1^{\text{in}}(50\text{ nM}) \cdot \left(\frac{50}{375}\right) = 0.0012\text{ min}^{-1} \qquad (25)$$

This value of k_1^{in}(375 nM) is the same value as used above for the 375 nM curve fit. We performed the curve fit adjustment before we realised that increasing DNA values increase the number of unspecific binding sites and actually decrease the probability of DNA cleavage. We believe that this is a relative strong argument for a random-access model, where hSMUG1 binds DNA randomly and not specifically. However, we only consider the model as semi-quantitative, because the experimental results determining reaction rates by gel data have considerable uncertainties.

Production of purified hSMUG1(25–270)

E. coli BL21(DE3) harbouring pETM-11-hSMUG1 which codes for a truncated and His-tagged wild-type protein [hSMUG1(25–270)-(His)×6-tag; consists of the amino acids 25–270], was grown in 400 ml auto-induced media containing kanamycin (50 µg/ml) at 28 °C for 24 h. The following procedures were performed at 4 °C or on ice. Cells were harvested by centrifugation, suspended in 25 ml lysis buffer (50 mM HEPES, pH 8.0, 300 mM NaCl, 5% (v/v) glycerol, 1 mM DTT, 1× Complete EDTA-free protease inhibitor cocktail) and lysed by the addition of 100 µg/ml lysozyme (final concentration) by incubation for 30 min at 4 °C with gentle shaking. The cell lysate was supplemented with 0.5% (v/v) Tergitol, 5 mM $MgCl_2$, 5 µg/ml DNase I and 5 µg/ml RNase A and incubated for an additional 30 min at 4 °C

with gentle shaking followed by centrifugation (10,000 g, 30 min). The clarified supernatant was applied to HisTrap HP (5 ml; GE Healthcare) and pre-equilibrated with buffer A (50 mM HEPES, pH 8.0, 300 mM NaCl) using a peristaltic pump. The following steps were performed using an ÄKTA™ start System (GE Healthcare) equilibrated with buffer A. The column was washed with 5% (v/v) of elution buffer B (buffer A containing 500 mM imidazole). For elution of hSMUG1(25–270)-(His)×6-tag, the 25–500 mM imidazole gradient of buffer B was applied to the column for 30 min with a fractionation speed of 1 ml/min. Fractions containing hSMUG1(25–270)-(His)×6-tag were pooled, supplemented with 50 µl of AcTEV protease (Thermo Fisher Scientific) in dialysis buffer (50 mM HEPES, 300 mM NaCl, 2 mM 2-mercaptoethanol) and incubated overnight. After the TEV protease treatment, the protein solution was applied to a HiTrap Talon 1 ml column (GE Healthcare) equilibrated with buffer A using Äkta™ start System. The untagged hSMUG1(25–270) was collected in the flow-through using a fraction size of 1 ml. The hSMUG1(25–270) was analysed with SDS-PAGE. The pure fractions were concentrated using Vivaspin 6 with molecular weight cut-off (MWCO) of 10,000 Da (Sartorius Stedim Biotech). The concentration was measured using the Pierce™ BCA Protein Assay Kit (Thermo Fisher Scientific) and the protein was stored at -20 °C in 50% (v/v) glycerol. The band from SDS-PAGE gel was analysed by MS that verified hSMUG1.

LEGEND TO FIGURES

Figure S1. Conversion of UIP to 3′-OH product by hAPE1. Substrate 1[^{32}P] (0.12 pmol) was incubated at 37 °C alone (lane 1), with EcUng (0.78 pmol) and hOGG1 (13 pmol) for 10 min (lane 2), with hSMUG1 (0.3 pmol) for 10 min (lane 3) or with hSMUG1 (0.3 pmol) for 30 min followed by purification of DNA on a column and incubation with hAPE1 (0.45 pmol) for 10 min (lane 4). Denaturing PAGE was performed on a 20% (w/v) minigel.

Figure S2. SDS-PAGE of purified hSMUG(25–270). Lane 2, fraction pool (4 µg) from the first HisTrap (5 ml) affinity chromatography step, which was treated with TEV protease and dialysed; lanes 3 and 4, fractions 3 and 5 (2 µg each), respectively, from the second HiTrap Talon crude (1 ml) affinity chromatography step to separate hSMUG(25–270) from His-tagged enzyme and TEV protease. The molecular weight marker (MWM; lane 1) is Precision Plus Protein™ Unstained Protein Standards (10 µl), Strep-tagged recombinant, from BioRad (product #1610363).

Figure S3. MALDI-TOF-MS signals for control incubation of U-DNA without enzyme. The lack of the MALDI-TOF-MS signal corresponding to UIP and UPP is indicated by comparing the analysis presented here with the analyses described in Figure 8A. Substrate (unlabelled substrate 2; Figure 8A) alone was incubated in 20 mM Tris-HCl, pH 8.0, 1 mM DTT, 1 mM EDTA, 70 mM KCl at 37 °C for 1 h.

Figure S4. MALDI-TOF-MS signals for incubation of U-DNA with hSMUG1 with and without hAPE1. hSMUG1 (0.3 pmol) was incubated with unlabelled substrate 2 (100 pmol) in 20 mM Tris-HCl, pH 8.0, 1 mM DTT, 1 mM EDTA, 70 mM KCl at 37 °C for 10 min, followed by incubation with (upper graph) and without (lower graph) hAPE1 (0.45 pmol) for 2 h. Following precipitation twice (before and after hAPE1 addition, in the presence of sodium acetate and ammonium acetate, respectively; see Materials and Methods), the DNA was dissolved in 10 µl water for MS analysis (200 ng/µl).

Figure S5. U-DNA incision rate of hSMUG1 (V^{in}; see Figure 9A) as a function of enzyme concentration $[E]_0$ at an initial U-DNA concentration $[S]_0$ of (**A**) 125 nM or (**B**) 375 nM, where incubation was performed for 20 min as described in Figure 4B. Each value represents the average (± SD) of 3–6 independent measurements.

REFERENCES

1. Asagoshi, K., Yamada, T., Terato, H., Ohyama, Y., Monden, Y., Arai, T., Nishimura, S., Aburatani, H., Lindahl, T. and Ide, H. (2000) Distinct repair activities of human 7,8-dihydro-8-oxoguanine DNA glycosylase and formamidopyrimidine DNA glycosylase for formamidopyrimidine and 7,8-dihydro-8-oxoguanine. *J Biol Chem*, **275**, 4956–4964.
2. Radicella, J.P., Dherin, C., Desmaze, C., Fox, M.S. and Boiteux, S. (1997) Cloning and characterization of *hOGG1*, a human homolog of the *OGG1* gene of *Saccharomyces cerevisiae*. *Proceedings of the National Academy of Sciences of the United States of America*, **94**, 8010–8015.
3. Bailly, V. and Verly, W.G. (1987) *Escherichia coli* endonuclease III is not an endonuclease but a β-elimination catalyst. *Biochem J*, **242**, 565–572.
4. Mazumder, A., Gerlt, J.A., Absalon, M.J., Stubbe, J., Cunningham, R.P., Withka, J. and Bolton, P.H. (1991) Stereochemical studies of the *β*-elimination reactions at aldehydic abasic sites in DNA: endonuclease III from *Escherichia coli*, sodium hydroxide, and Lys-Trp-Lys. *Biochemistry*, **30**, 1119–1126.
5. Piersen, C.E., McCullough, A.K. and Lloyd, R.S. (2000) AP lyases and dRPases: commonality of mechanism. *Mutat Res*, **459**, 43–53.
6. Chung, S.J. and Verdine, G.L. (2004) Structures of end products resulting from lesion processing by a DNA glycosylase/lyase. *Chem Biol*, **11**, 1643–1649.
7. Fromme, J.C. and Verdine, G.L. (2003) Structure of a trapped endonuclease III–DNA covalent intermediate. *EMBO J*, **22**, 3461–3471.
8. McCullough, A.K., Sanchez, A., Dodson, M.L., Marapaka, P., Taylor, J.S. and Lloyd, R.S. (2001) The reaction mechanism of DNA glycosylase/AP lyases at abasic sites. *Biochemistry*, **40**, 561–568.
9. Fromme, J.C. and Verdine, G.L. (2003) Structure of a trapped endonuclease III-DNA covalent intermediate. *EMBO J*, **22**, 3461–3471.
10. Bjørås, M., Luna, L., Johnsen, B., Hoff, E., Haug, T., Rognes, T. and Seeberg, E. (1997) Opposite base-dependent reactions of a human base excision repair enzyme on DNA containing 7,8-dihydro-8-oxoguanine and abasic sites. *EMBO J*, **16**, 6314–6322.
11. Sun, B., Latham, K.A., Dodson, M.L. and Lloyd, R.S. (1995) Studies on the catalytic mechanism of five DNA glycosylases. Probing for enzyme-DNA imino intermediates. *J Biol Chem*, **270**, 19501–19508.
12. Darwanto, A., Farrel, A., Rogstad, D.K. and Sowers, L.C. (2009) Characterization of DNA glycosylase activity by matrix-assisted laser desorption/ionization time-of-flight mass spectrometry. *Anal Biochem*, **394**, 13–23.
13. Castellan, G.W. (1983) *Physical Chemistry*. 3 ed. Addison-Wesley, Reading, Massachusetts.

Table S1. MS analysis of commercial hSMUG1 preparation

Checked	Master	Accession	Description	Coverage	# Peptides	# PSMs	# Unique Peptides	# Protein Groups	# AAs	MW [kDa]	calc. pI	Protein FDR Confidence	Mascot Exp. q-value	Mascot Score	Mascot # Peptides
USANN	Master	Protein P02769	Serum albumin OS=Bos taurus GN=ALB PE=1 SV=4	77,59472817	57	589	42	1	607	69,248	6,18	High	0	17160,79704	57
USANN	Master	Protein P08835	Serum albumin OS=Sus scrofa GN=ALB PE=1 SV=2	17,6276771	13	123	1	1	607	69,647	6,49	High	0	2879,437004	13
USANN	Master	Protein P49822	Serum albumin OS=Canis lupus familiaris GN=ALB PE=1 SV=3	11,34868421	9	98	1	1	608	68,56	5,69	High	0	2348,265297	9
USANN	Master	Protein P02768	Serum albumin OS=Homo sapiens GN=ALB PE=1 SV=2	9,688013136	7	77	2	1	609	69,321	6,28	High	0	1658,559994	7
USANN	Master	Protein Q53HV7	Single-strand selective monofunctional uracil DNA glycosylase OS=Homo sapiens GN=SMUG1 PE=1 SV=2	59,25925926	13	55	9	1	270	29,842	6,62	High	0	1485,567343	13
USANN	Master	Protein P04264	Keratin, type II cytoskeletal 1 OS=Homo sapiens GN=KRT1 PE=1 SV=6	29,34782609	14	28	12	1	644	65,999	8,12	High	0	1056,903975	14
USANN	Master	Protein P00761	Trypsin OS=Sus scrofa PE=1 SV=1	25,10822511	4	28	4	1	231	24,394	7,18	High	0	736,6334541	4
USANN	Master	Protein P13645	Keratin, type I cytoskeletal 10 OS=Homo sapiens GN=KRT10 PE=1 SV=6	35,2739726	16	23	13	1	584	58,792	5,21	High	0	645,6170418	16
USANN	Master	Protein P49065	Serum albumin OS=Oryctolagus cuniculus GN=ALB PE=1 SV=2	10,36184211	8	22	2	1	608	68,865	6,24	High	0	501,912621	8
USANN	Master	Protein P35908	Keratin, type II cytoskeletal 2 epidermal OS=Homo sapiens GN=KRT2 PE=1 SV=2	31,14241002	14	17	9	1	639	65,393	8	High	0	437,6774163	14
USANN	Master	Protein P02538	Keratin, type II cytoskeletal 6A OS=Homo sapiens GN=KRT6A PE=1 SV=3	29,96453901	16	16	3	1	564	60,008	8	High	0	417,460209	16
USANN	Master	Protein P35527	Keratin, type I cytoskeletal 9 OS=Homo sapiens GN=KRT9 PE=1 SV=3	30,33707865	12	13	11	1	623	62,027	5,24	High	0	412,2821524	12
USANN	Master	Protein P04259	Keratin, type II cytoskeletal 6B OS=Homo sapiens GN=KRT6B PE=1 SV=5	25,35460993	14	15	1	1	564	60,03	8	High	0	356,1471413	14
USANN	Master	Protein Q6PSC5	Single-strand selective monofunctional uracil DNA glycosylase OS=Mus musculus GN=Smug1 PE=1 SV=1	20,43010753	5	16	1	1	279	30,635	6,77	High	0	355,1021782	5
USANN	Master	Protein P08779	Keratin, type I cytoskeletal 16 OS=Homo sapiens GN=KRT16 PE=1 SV=4	22,62156448	10	13	4	1	473	51,236	5,05	High	0	283,5066545	10
USANN	Master	Protein Q3SZR3	Alpha-1-acid glycoprotein OS=Bos taurus GN=ORM1 PE=2 SV=1	31,68316832	7	9	7	1	202	23,168	5,87	High	0	262,9563804	7
USANN	Master	Protein P02533	Keratin, type I cytoskeletal 14 OS=Homo sapiens GN=KRT14 PE=1 SV=4	23,51694915	10	13	3	1	472	51,529	5,16	High	0	252,2528084	10
USANN	Master	Protein A5A6M8	Keratin, type II cytoskeletal 5 OS=Pan troglodytes GN=KRT5 PE=2 SV=1	15,87837838	10	10	5	1	592	62,5	7,3	High	0	173,1344831	10
USANN	Master	Protein Q04695	Keratin, type I cytoskeletal 17 OS=Homo sapiens GN=KRT17 PE=1 SV=2	18,51851852	7	9	3	1	432	48,076	5,02	High	0	163,0714326	7
USANN	Master	Protein Q2UVX4	Complement C3 OS=Bos taurus GN=C3 PE=1 SV=2	2,046959663	3	3	3	1	1661	187,135	6,84	High	0	120,7966667	3
USANN	Master	Protein P41361	Antithrombin-III OS=Bos taurus GN=SERPINC1 PE=1 SV=2	4,946236559	2	3	2	1	465	52,314	7,33	High	0	82,02	2
USANN	Master	Protein P01030	Complement C4 (Fragments) OS=Bos taurus GN=C4 PE=1 SV=2	2,608695652	2	2	2	1	920	101,817	6,58	High	0	73,82	2
USANN	Master	Protein P50448	Factor XIIa inhibitor OS=Bos taurus PE=1 SV=1	2,564102564	1	1	1	1	468	51,691	6,67	High	0	70,76	1

Figure S1

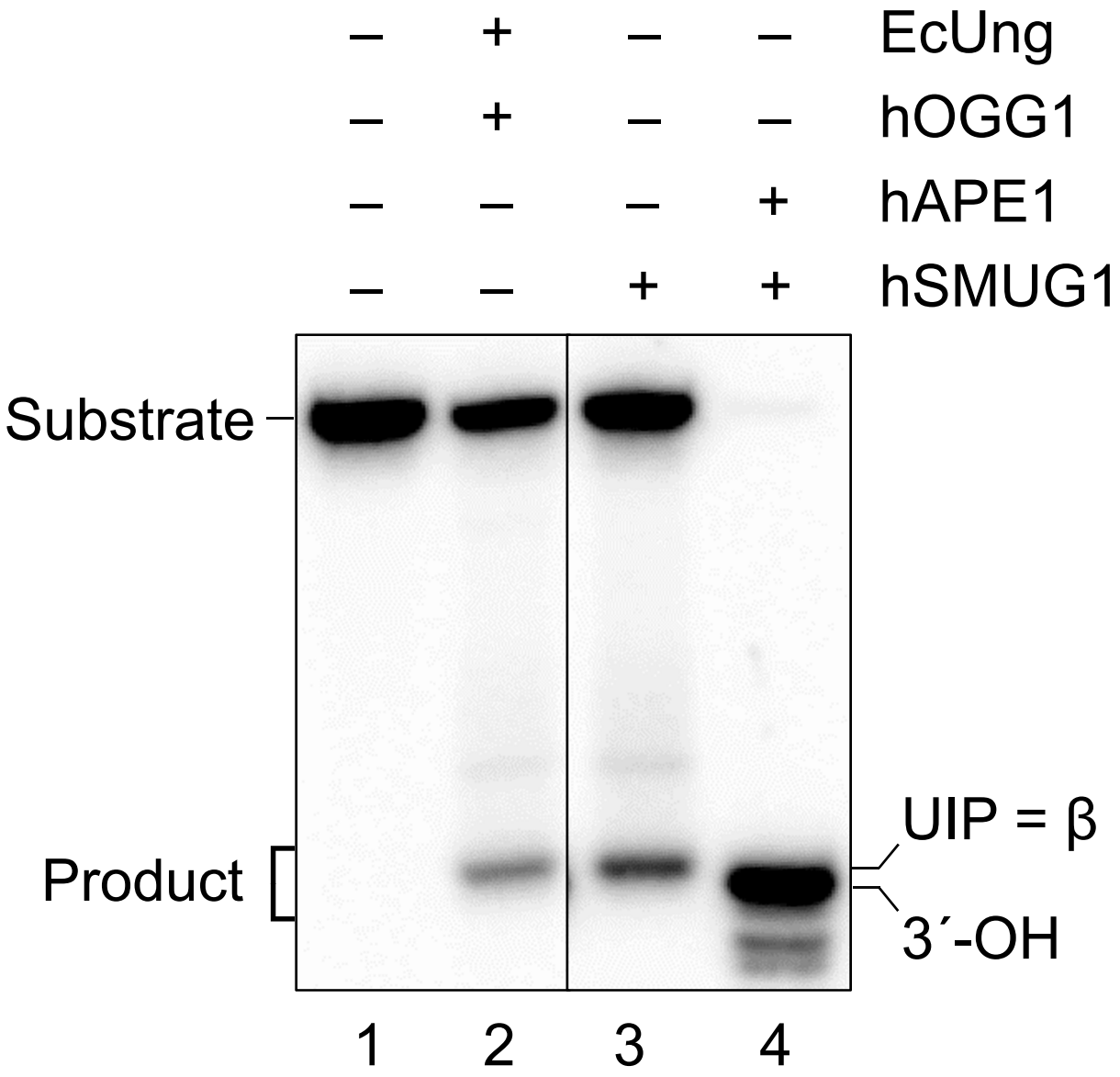

Figure S2

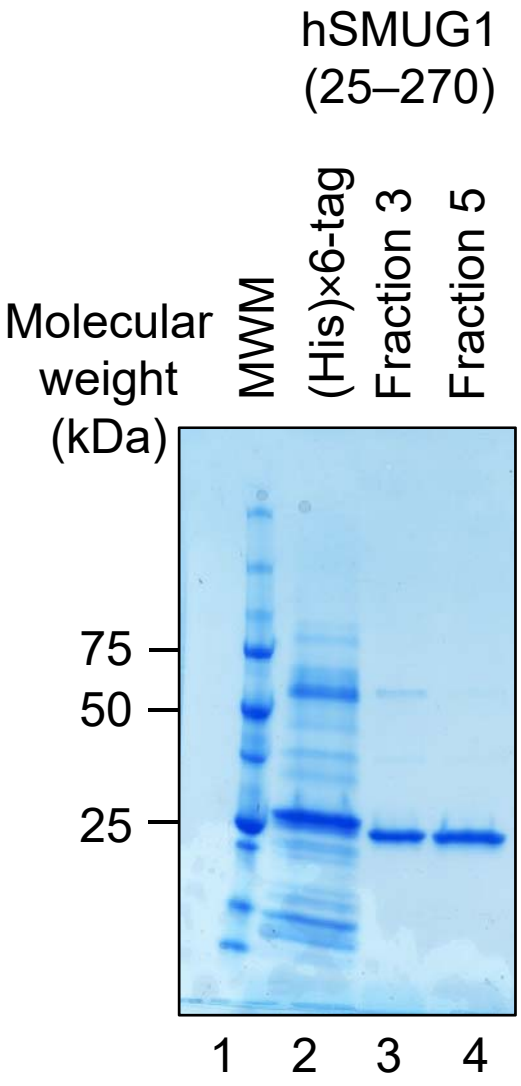
hSMUG1
(25–270)
Molecular
weight
(kDa)
MWM
(His)×6-tag
Fraction 3
Fraction 5
75
50
25
1
2
3
4

Figure S3

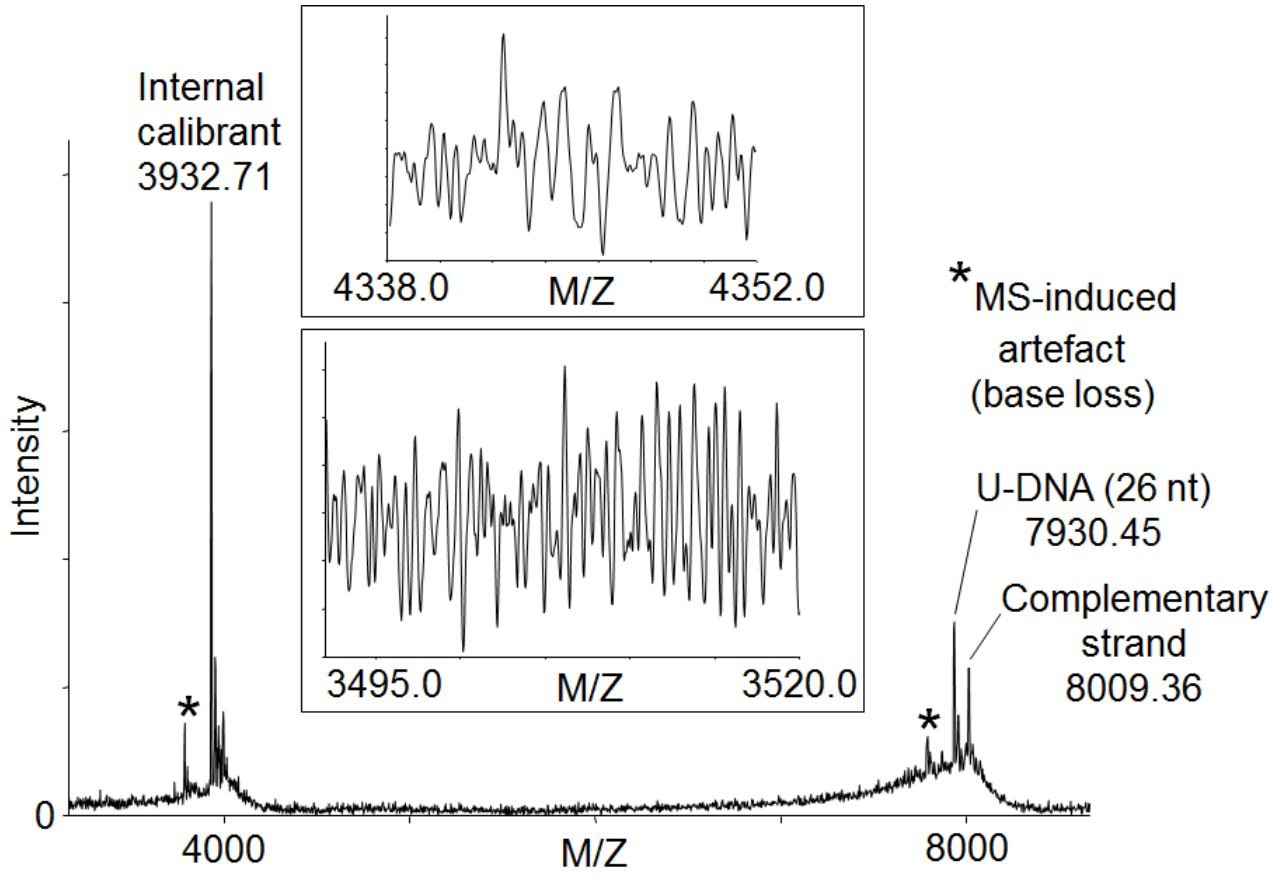
Internal
calibrant
3932.71
4338.0
M/Z
4352.0
3495.0
M/Z
3520.0
*MS-induced
artefact
(base loss)
U-DNA (26 nt)
7930.45
Complementary
strand
8009.36
Intensity
0
4000
M/Z
8000

Figure S4

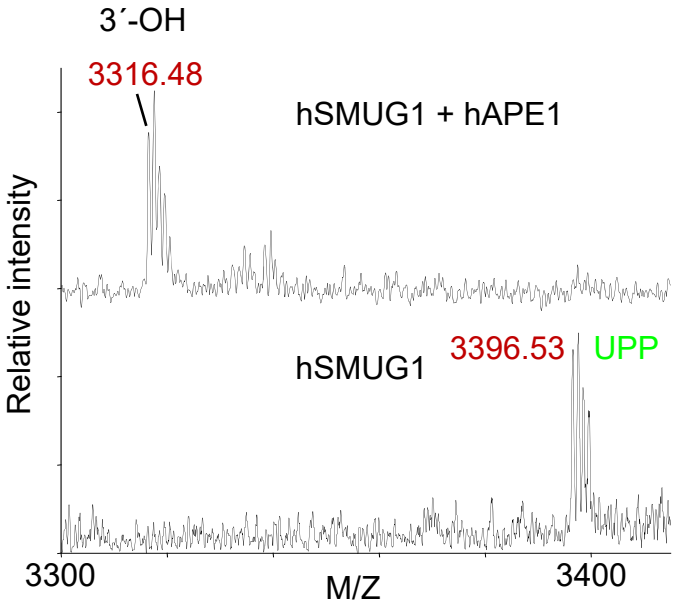
3´-OH
3316.48
hSMUG1 + hAPE1
Relative intensity
hSMUG1
3396.53
UPP
3300
M/Z
3400

Figure S5

A

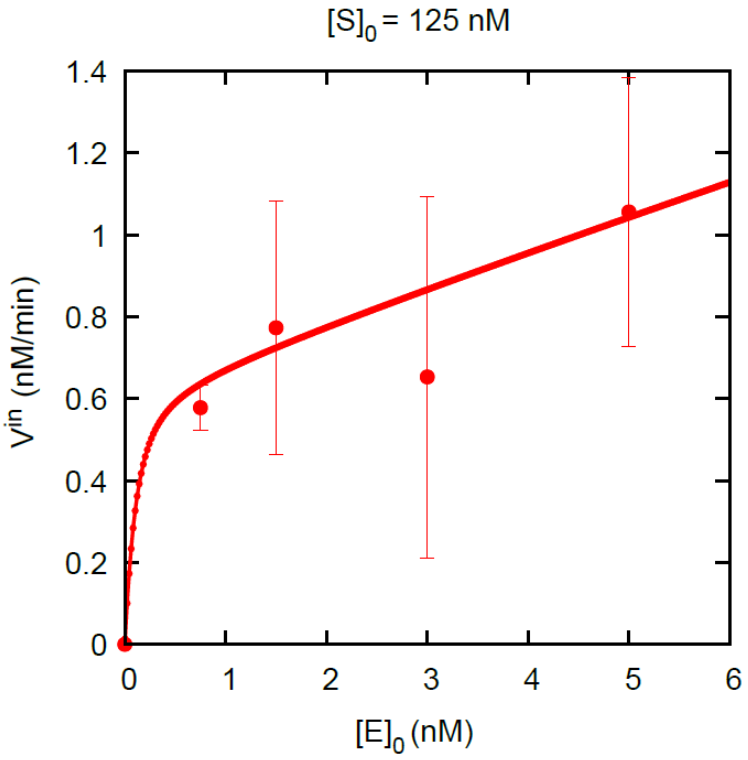
[S]0 = 125 nM
Vin (nM/min)
[E]0 (nM)
0
0.2
0.4
0.6
0.8
1
1.2
1.4
0
1
2
3
4
5
6

B

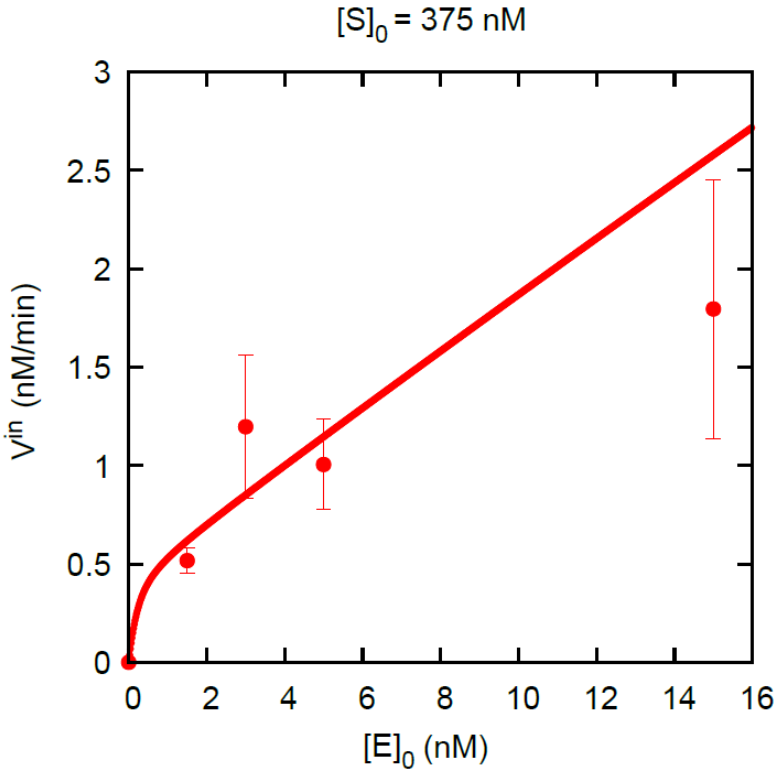
[S]0 = 375 nM
Vin (nM/min)
[E]0 (nM)
0
0.5
1
1.5
2
2.5
3
0
2
4
6
8
10
12
14
16